UNIVERSITY OF MINNESOTA
ST. ANTHONY FALLS HYDRAULIC LABORATORY

Project Report No. 252

HYDRODYNAMIC ANALYSIS OF THE SSL FLOW FACILITY

by

Charles C. S. Song

Mingshun Yuan

Joseph M. Wetzel

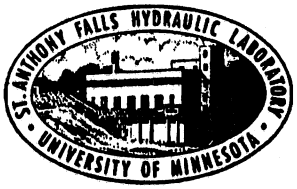

Prepared for

David Taylor Naval Ship Research & Development Center
Washington, D. C.

Contract No. N00014-85-K-0265

March, 1987
Minneapolis, Minnesota

TABLE OF CONTENTS

LIST OF FIGURES

Hydrodynamic Analysis of the SSL Flow Facility

I. INTRODUCTION

A preliminary concept for a gravity flow test facility was evaluated using mathematical modeling techniques. Complete specifications for the hydrodynamic performance were not available. In the absence of these values, parametric studies were carried out to determine the sensitivity of flow quality indicators to dimensional changes. The target flow conditions in a circular test section with a 4 sq ft area were a 90 second test run at a constant velocity of 60 fps.

A transient analysis indicated that such a flow could be established within the constraints of the preliminary concept. Required valve opening characteristics were defined to initiate and maintain the flow under a falling head.

The preliminary concept of the facility employed a bottom outlet in the head tank. This required a vaned elbow to divert the flow through a contraction into the horizontal test section. Although a contraction shape was selected and analysed for use in this configuration, it appeared that a side outlet should also be investigated, as the vaned elbow could then be omitted. A rather extensive parametric study was performed to determine the optimum dimensions for the side outlet. The design was evaluated on the basis of uniformity of test section velocity distribution and freedom of boundary layer separation.

With a gravity flow system, the pressure in the test section did not remain constant with time. To increase the flexibility of facility usage, it was suggested that the test section pressure also be controllable. This can be accomplished through use of a pneumatic drive system for which the pressure above the water surface in the head and tail tanks is variable. A preliminary analysis of the operation of a pneumatic drive system was made to assess its practicality.

The methods used in the mathematical modeling and the results obtained are discussed in the sections below, and recommendations are made for the flow facility. Some of the features may require modification depending on a more complete definition of the test requirements.

II. DESCRIPTION OF MATHEMATICAL MODELS

A. One-Dimensional Transient Flow Model

The detailed procedure for the establishment and maintenance of desired flow conditions at the test section was studied with a one-dimensional transient flow model. The objective was to determine the necessary characteristics and the operating procedure of a control valve which will generate the desired flow at the test section. A schematic of the tunnel analyzed is shown in Fig. 1.

The governing equations are

$$\frac{\partial H}{\partial t} + \frac{a^2}{gA}\frac{\partial Q}{\partial x} = 0 \tag{1}$$

$$\frac{\partial Q}{\partial t} + gA\frac{\partial H}{\partial x} + f\frac{Q|Q|}{2DA} = 0 \tag{2}$$

in which $H = \frac{v^2}{2g} + \frac{P}{\gamma} + z$ = total head

Q = discharge

a = speed of waterhammer wave

g = gravitational acceleration

A = cross-sectional area

D = diameter

f = friction coefficient

The governing equations are solved by the method of characteristics in a fixed grid system. The two sets of characteristic equations are

$$C^+, \qquad \frac{dx}{dt} = a$$

$$\frac{dH}{dt} + \frac{a}{gA}\frac{dQ}{dt} + \frac{faQ|Q|}{2g\,DA^2} = 0 \tag{3}$$

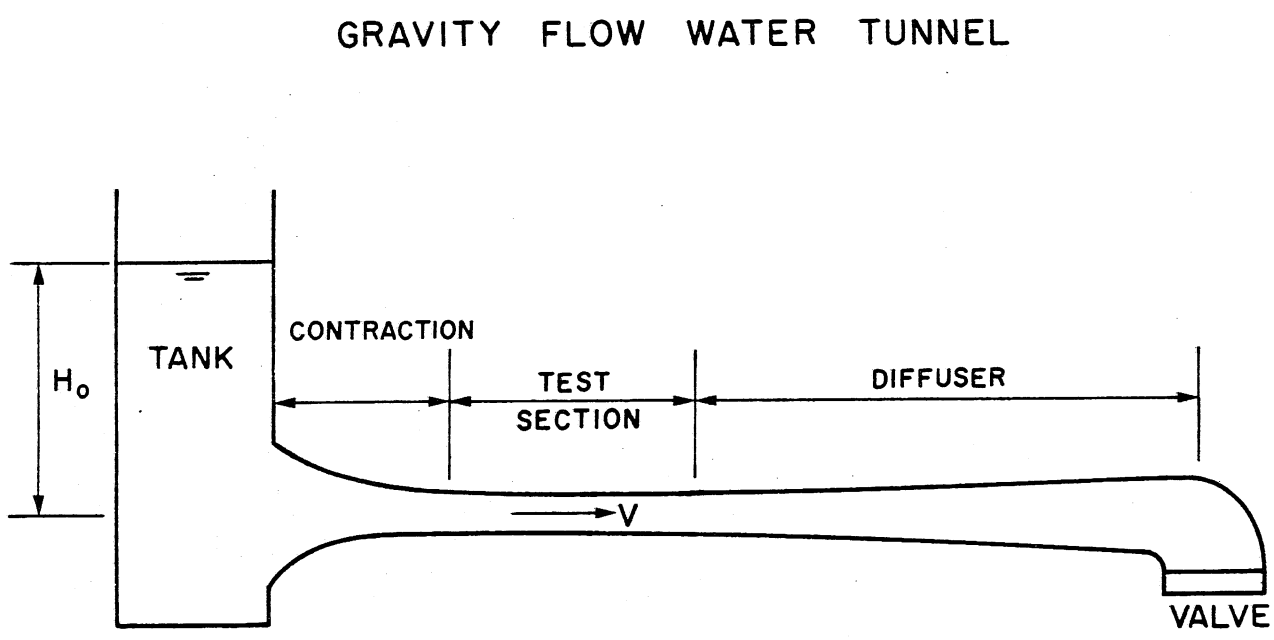

Figure 1. Schematic of gravity flow water tunnel.

$$C^-, \qquad \frac{dx}{dt} = -a$$

$$-\frac{dH}{dt} + \frac{a}{gA}\frac{dQ}{dt} + \frac{faQ|Q|}{2g\ DA^2} = 0 \tag{4}$$

The above sets of characteristic equations are solved explicitly on the x-t plane with a fixed grid system as shown in Fig. 2.

The vertical line $\overline{A_1A_2}$ in Fig. 2 represents the upstream end of the tunnel where the total head is assumed to be equal to the elevation of the water surface H_o. This water surface elevation changes with time as water flows out of the tank. The rate of change of the water surface elevation is related to the flow rate by

$$A_o \frac{dH_o}{dt} + Q = 0 \tag{5}$$

in which A_o is the cross-sectional area of the storage tank.

The vertical line $\overline{B_1B_2}$ in Fig. 2 represents the middle of the test section where the velocity will increase rapidly from zero to a specified test velocity and, thereafter, maintain a constant value for a prescribed period of time. Thus a boundary condition of the following form is given on $\overline{B_1B_2}$.

$$Q = Q(t) \tag{6}$$

The line $\overline{C_1C_2}$ is the downstream end of the tunnel located just upstream of the control valve where both Q and H are unknown.

In summary the numerical problem is to solve Eqs. 3 and 4 for Q and H for all the grid points on the x-t plane subject to the boundary conditions, Eqs. 5 and 6. The control valve and its operating procedure are determined based on the required Q and H at the downstream end.

To solve the numerical problem, the x-t plane is first divided into two regions, $A_1A_2B_2B_1$ and $B_1B_2C_2C_1$. We have a standard boundary value-initial value problem in region $A_1A_2B_2B_1$. Any interior point P_1 shown in Fig. 2 may be calculated by solving two appropriate characteristic equations. Any boundary point on $\overline{A_1A_2}$ can be calculated by solving the C^- equation and Eq. 5. A point on $\overline{B_1B_2}$ is calculated by the C^+ equation and Eq. 6. Thus the problem in the first region is a direct problem which can be solved completely, including the boundary $\overline{B_1B_2}$, by marching forward in time.

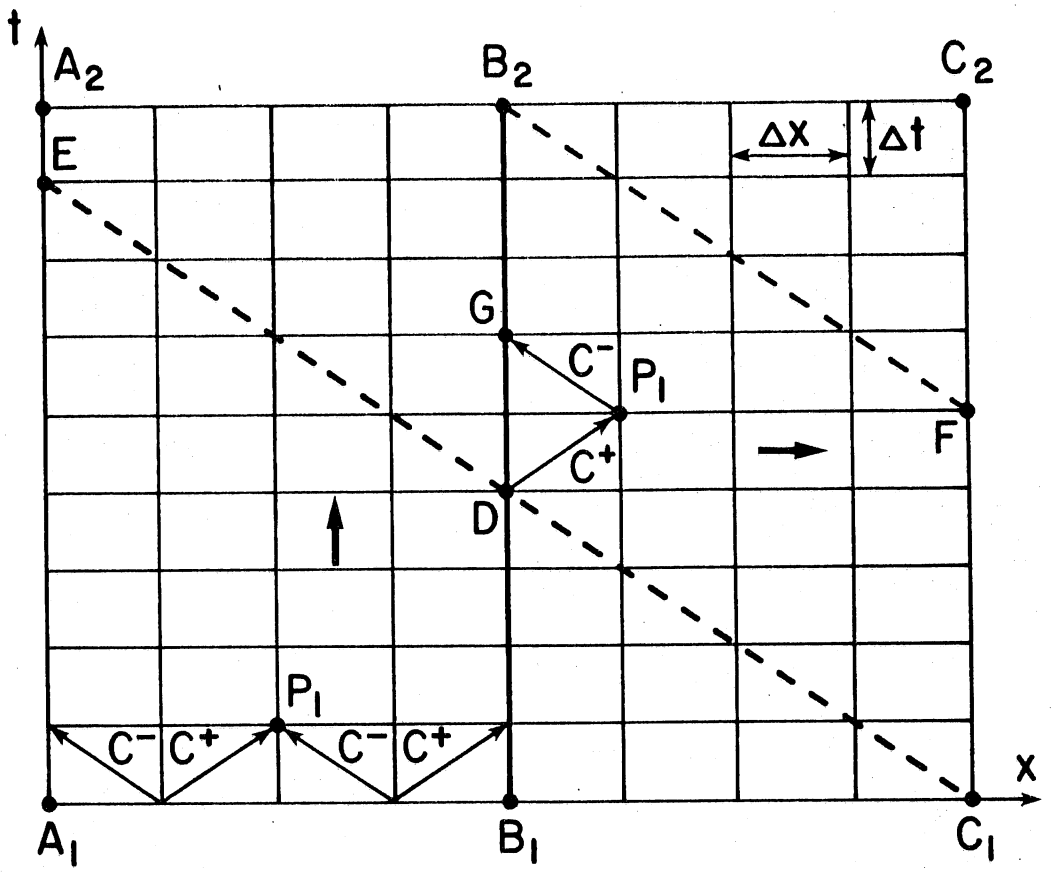

Figure 2. The fixed-grid x-t plane.

After the solution in the first region is completed, the problem for the second region becomes that of a semi-inverse problem wherein the complete set of (Q, H) variables are given on $\overline{B_1C_1}$ and the upstream boundary $\overline{B_1B_2}$. If the initial condition is static and the flow is set up by the valve starting its motion at t=0, then the dynamic condition exists only above the dotted lines $\overline{C_1DE}$. In this case, velocity is zero on $\overline{B_1D}$, and nonzero velocity may be specified on $\overline{DB_2}$. According to Fig. 2, only the valve movement on $\overline{C_1F}$ determines the flow on $\overline{DB_2}$. Thus, only the region bounded by C_1DB_2F needs to be computed. A typical interior point P_2 possesses a forward characteristic equation C^+ and a backward characeristic equation C^-. In otherwords, the flow at P_2 is determined by a previous condition at D and a future condition at G. If the backward characteristic equation causes no numerical instability then the computation can proceed from left to right. Since viscous flow is an irreversible system an inverse problem may not necessarily have a unique solution.

B. Contraction

1. Governing Equations

A three-dimensional flow model is required to calculate the flow in the tank and the contraction. A previously developed "weakly compressible Euler equations model" was used for this purpose. This model is a three-dimensional version of the hydraulic transient flow model which can be used to compute three-dimensional steady and unsteady flows at small Mach numbers. At a small Mach number, only the equation of continuity contributes the first order effect of compressiiblity.

Based on the relationship,

$$a^2 = \frac{\partial P}{\partial \rho} \tag{7}$$

where a is the speed of sound, the equation of continuity may be written as

$$\frac{\partial P}{\partial t} + a^2 \nabla \cdot \rho \vec{V} = 0 \tag{8}$$

For small Mach numbers, a is nearly constant and Eq. 8 is simplified to

$$\frac{\partial P}{\partial t} + \nabla \cdot K\vec{V} = 0 \tag{9}$$

where $K = a^2\rho$ (10)

is the bulk modulus of elasticity. The equation of motion for the weakly compressible flow whose accuracy is up to the first order of Mach number is identical to that of the incompressible flow.

The conservative form of the governing equations of weakly compressible, nonviscous flow is

$$\frac{\partial U}{\partial t} + \nabla \cdot \vec{F} = 0 \tag{11}$$

where $$\vec{F} = iE + jF + kG \tag{12}$$

$$U = \left[P,\ u,\ v,\ w\right]^T \tag{13}$$

$$E = \left[Ku,\ u^2 + \frac{P}{\rho},\ uv,\ uw\right]^T \tag{14}$$

$$F = \left[Kv,\ uv,\ v^2 + \frac{P}{\rho},\ vw\right]^T \tag{15}$$

$$G = \left[Kw,\ uw,\ vw,\ w^2 + \frac{P}{\rho} + gz\right] \tag{16}$$

In writing the above equations, gravity is assumed to act in the negative z-direction.

2. Finite Volume Method

This model adopts the finite volume approach which is quite popular in aerodynamic computations. Equation 11 is first integrated over a finite volume $\Delta\forall$, and by applying the divergence theorem to obtain

$$\frac{\partial \overline{U}}{\partial t} + \frac{1}{\Delta\forall}\int_A \vec{n}\cdot\vec{F}\, dA = 0 \tag{17}$$

In the above equation, $\overline{U}$ is the mean value of U within the finite volume and the integral is the flux of $\vec{F}$ through the boundary surface A of the finite volume. $\vec{n}$ is a unit normal vector on A which is positive when pointing outward.

MacCormack's predictor-corrector method is used to solve Eq. 17. This method is briefly explained as follows. First Eq. 17 is represented in the following form.

$$\frac{\partial \overline{U}}{\partial t} = H \tag{18}$$

Let n and n+1 represent, respectively, the beginning and the end of a time step. Knowing the flow at time n, the value at time n+1 is first predicted by the following finite difference expression of Eq. 18.

$$\hat{U}^{n+1} = \bar{U}^{n} + H^{n}\Delta t \tag{19}$$

Using the predicted value of $\hat{U}^{n+1}$, the predicted flux $\hat{H}^{n+1}$ may be computed. The corrected value of $\bar{U}^{n+1}$ is given by

$$\bar{U}^{n+1} = \bar{U}^{n} + \frac{H^{n} + \hat{H}^{n+1}}{2}\Delta t \tag{20}$$

The corrected value H^{n+1} may be computed using $\bar{U}^{n+1}$.

3. Solid Surface Boundary Condition

In computing the flux out of a finite volume, it is necessary to use the value of $\vec{F}$ of the neighboring volumes. For a volume next to a solid boundary there is missing a real finite volume because there is no fluid outside of the boundary. A scheme based on a phantom volume as illustrated in Fig. 3 is used. For the sake of simplicity, only a two-dimensional case is shown here.

The boundary volume 1 is the volume for which computation is to be performed. Volumes 2, 3, and 4 are the neighboring volumes within the flow field and volume P is the phantom volume. To complete the computation for volume 1 it is necessary to know $\bar{U}$ at P. For nonviscous fluid it is customary to assume the perfect slip condition on the solid boundary. This boundary condition specifies the velocity at P as

$$\vec{V}_P = \vec{V}_1 - 2\vec{n}\cdot\vec{V}_1 \tag{21}$$

For the numerical scheme to work, it is also necessary to specify the pressure on the phantom volume because it is needed to calculate the flow values at volume 1. Because this would result in theoretical over specification of boundary conditions, the pressure specified at P must be compatible with the governing equations. If the grids are extremely small, then it is sufficient to assume

$$P_p = P_1 \tag{22}$$

However, Eq. 22 may result in inacceptable error due to the existence of a pressure gradient in the direction normal to the surface, if the grid size is not much smaller than the radius of curvature of the streamline. In this case the refined boundary condition is

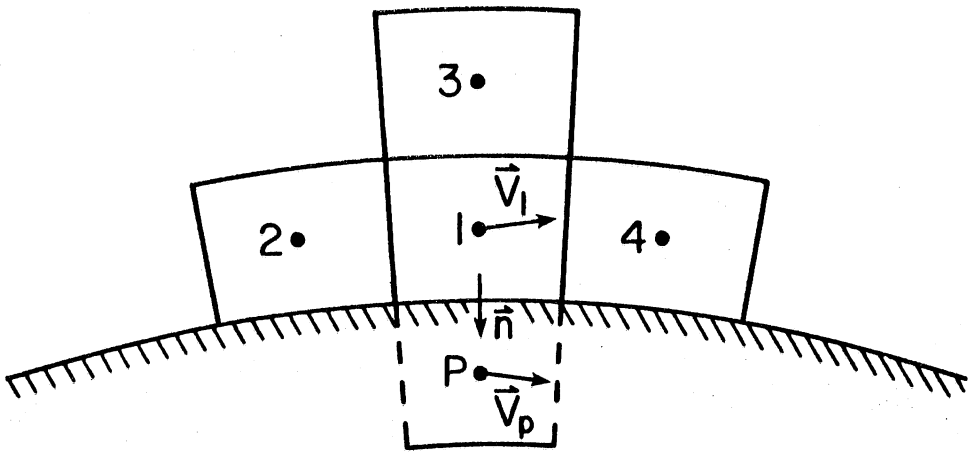

Figure 3. Plantom volume and solid surface boundary condition.

$$P_p = P_1 - \rho V_1^2 \frac{\Delta n}{r} \tag{23}$$

in which Δn is the distance between 1 and P and r is the radius of curvature of the boundary.

4. Free-Surface Boundary Condition

A free-surface boundary condition is needed to represent the water surface in the storage tank. Because the free-surface boundary moves as water is drained from the tank, it is not convenient to use a boundary fitted grid system. The geometry of the three-dimensional flow field is quite complex and it is very time consuming to recalculate the grid system from time to time as the water drains from the tank. For this reason, a fixed-grid system established at t=0 is used for all subsequent computations.

Figure 4 shows a typical configuration of the fixed-grid system and the free-surface. The position of the free-surface at any instant must be determined by tracking its movement. As shown in Fig. 4, if grid 1 is more than half filled with water, then it is considered a boundary grid. In this case grid P becomes the corresponding phantom grid. If more than half of this grid is empty, then this grid becomes a phantom grid and grid 3 becomes a boundary grid. The boundary conditions are

$$\vec{V}_p = \vec{V}_1 \tag{24}$$

$$P_p = P_1 - \rho g(\Delta z_1 + \Delta z_p) \tag{25}$$

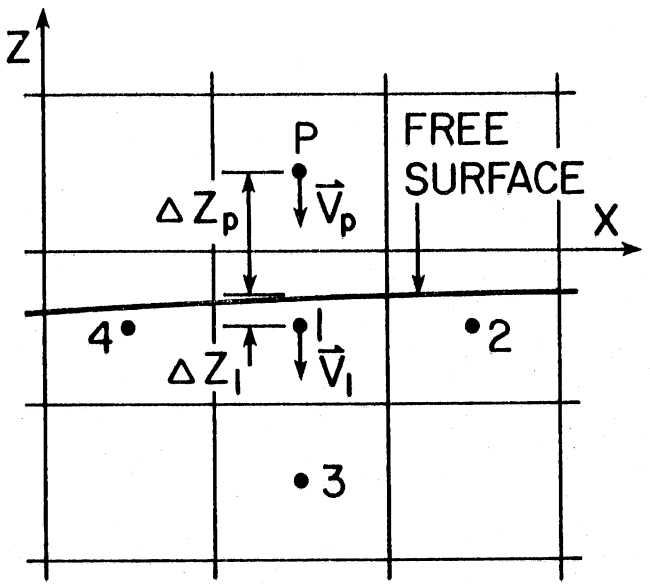

Figure 4. Free-surface boundary with a fixed-grid system.

III. DISCUSSION OF RESULTS

A. Transient Analysis - Flow Control

The purpose of this analysis is to find a valve operating characteristic that will produce a desired velocity at the test section for a certain time period without producing undesirable pressure and velocity fluctuations. Referring to Fig. 2, the velocity at the test section may be specified on line $\overline{DB}_2$ in many different ways.

The first few runs were made for the case when the velocity at the test section was increased linearly from zero to 60 fps within a specified time interval T_1 and then kept constant thereafter. Different ramp times, T_1 , were tried.

Figures 5 and 6 show the results of the case when T_1 is 10 seconds. The dotted line in Fig. 5 is the input data indicating the way velocity at the test section is varied with time. The broken line shows the way the valve coefficient C_v must be varied to achieve the specified velocity change. Here the valve coefficient is defined in the following way:

$$Q = C_v\sqrt{H} \tag{26}$$

Observe the existence of a small kink in the C_v diagram near the time of 10 seconds. This C_v overshoot, which increases with decreasing T_1 , makes the valve operation difficult. Another undesirable result of this run is the high frequency pressure oscillation at the test section generated by the sudden valve motion at the beginning and the end of velocity ramping (see Fig. 6).

To improve the performance of the flow control, the velocity at the test section was specified to vary smoothly as expressed by the following equation.

$$V = \frac{t^2}{T_1^2}\left(3 - 2\,\frac{t}{T_1}\right)V_o \tag{27}$$

In the above equation V_o is the desired constant velocity at the test section. Note that Eq. 27 gives zero rate of velocity change at both ends of T_1 . The computed results for the T_1 = 10 second case are shown in Figs. 7 and 8. These figures show that the required valve movement is very smooth and there is no pressure oscillation at the test section. Figure 8 shows that the test section pressure gradually decreases after the first 10 seconds as the water is gradually drained from the storage tank.

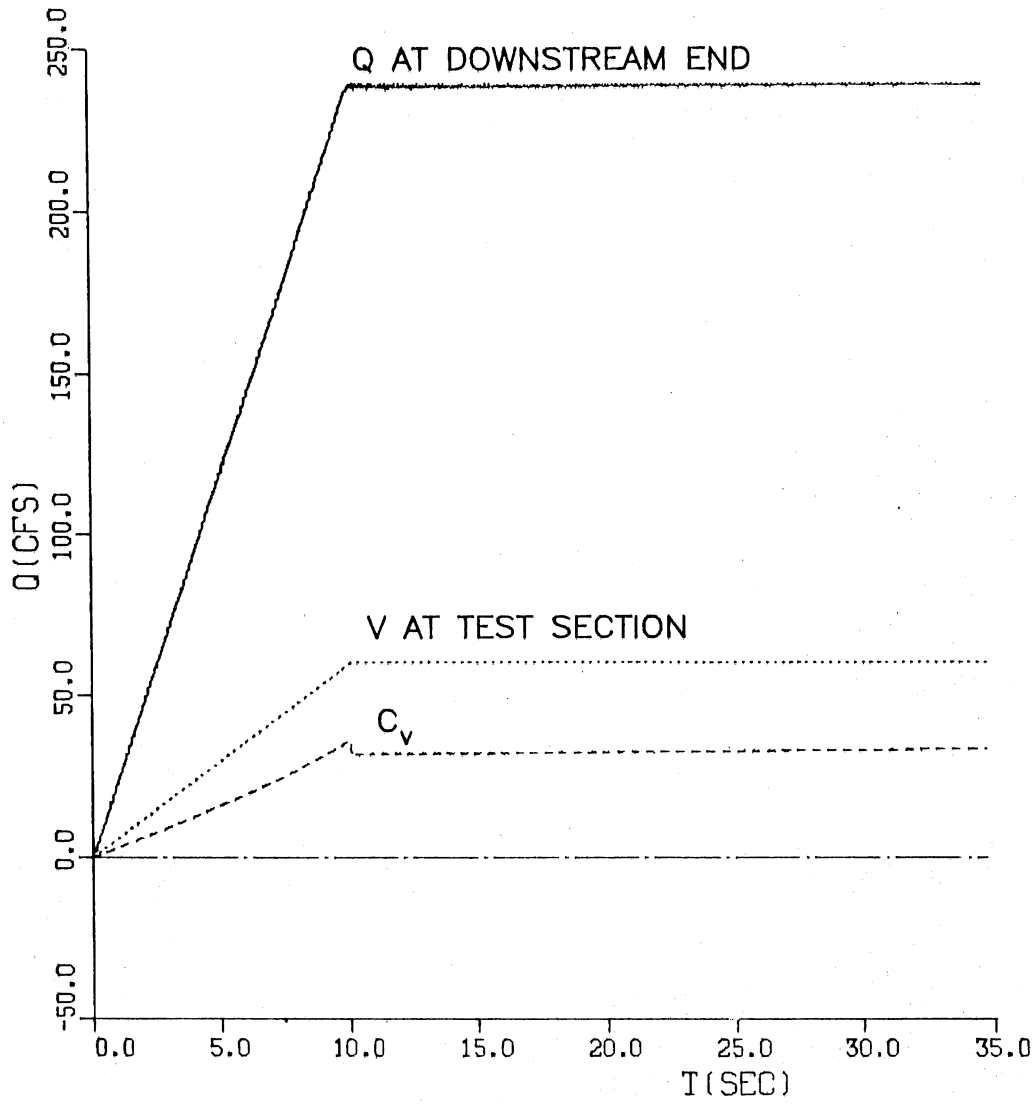

Figure 5. Hydraulic transients when velocity at test section increases linearly to 60 fps in 10 seconds.

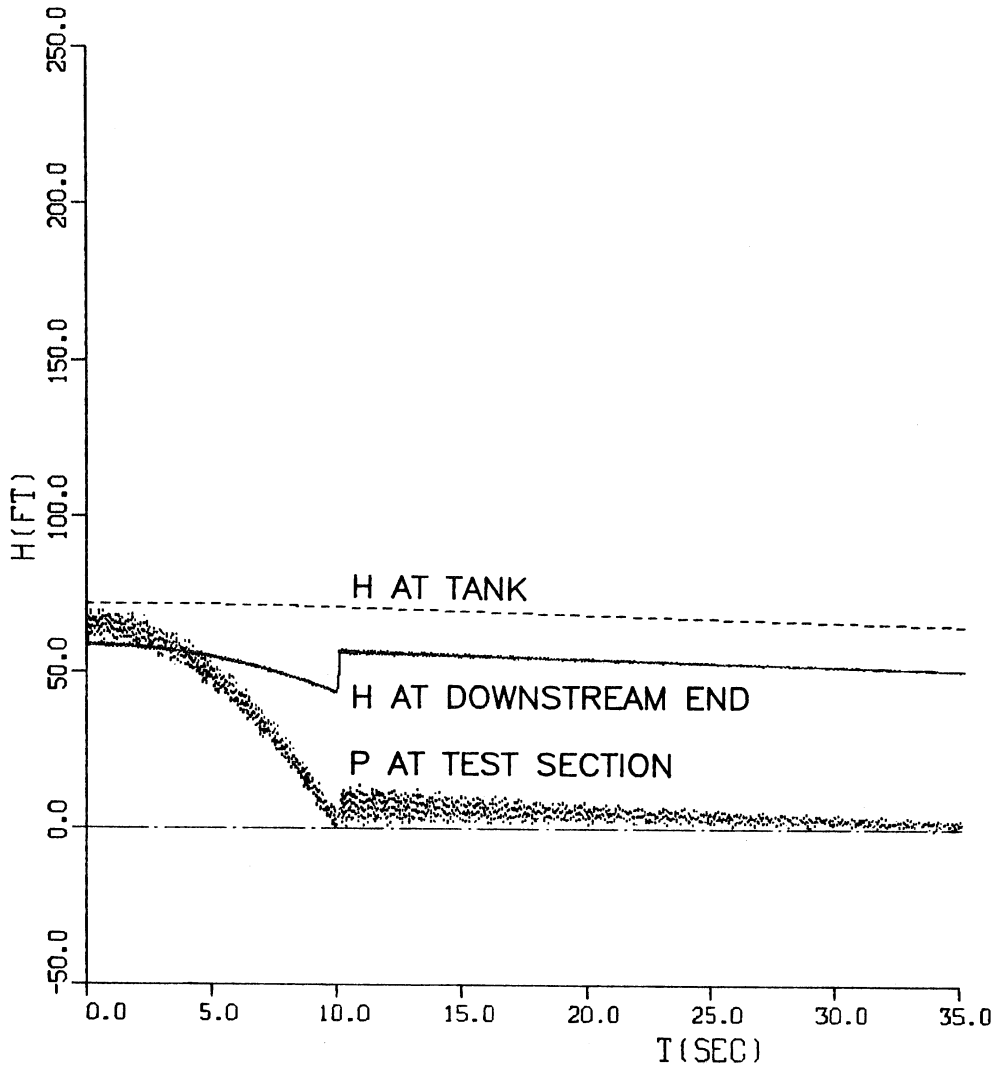

Figure 6. Hydraulic transients when velocity at test section increases linearly to 60 fps in 10 seconds.

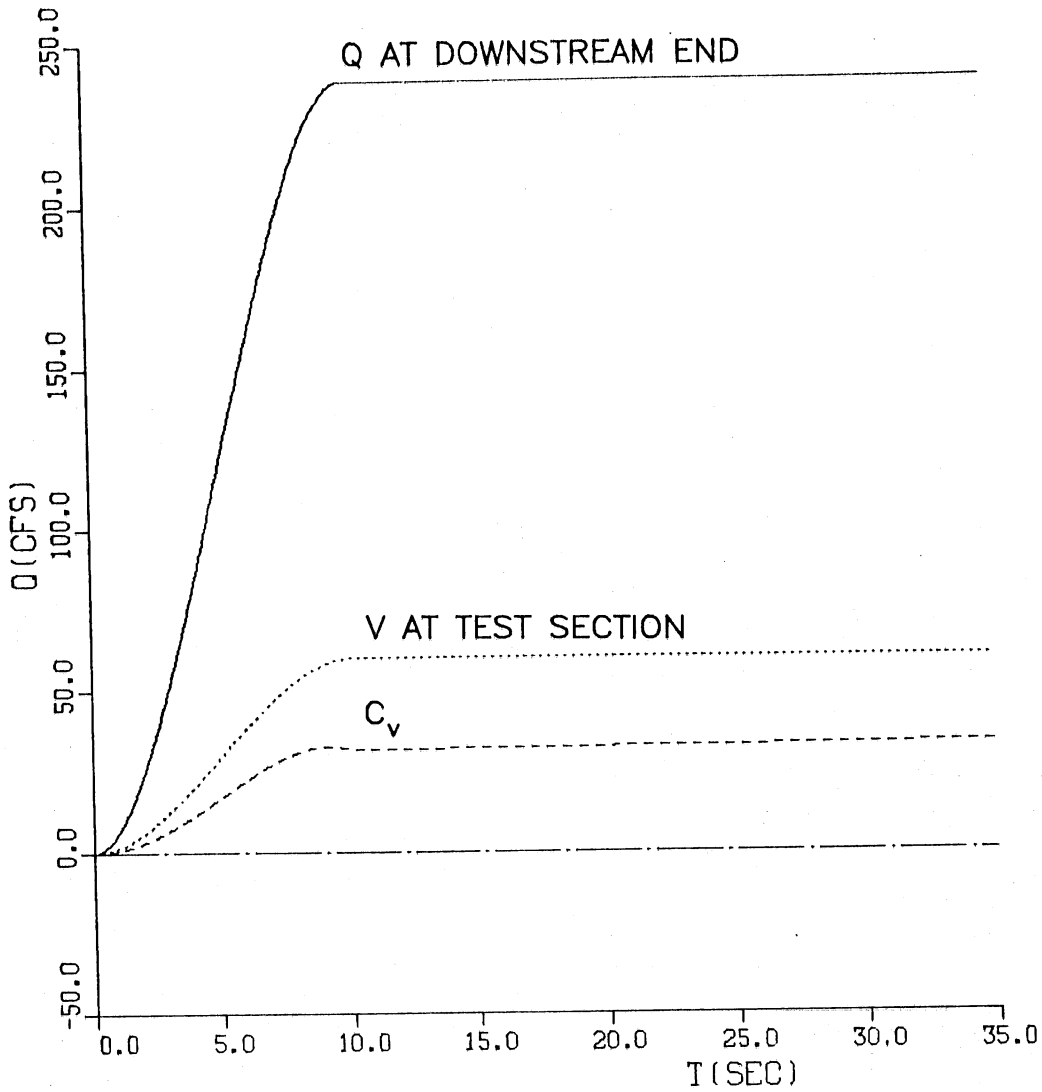

Figure 7. Hydraulic transient when the test section velocity is increased with continuous rate of change.

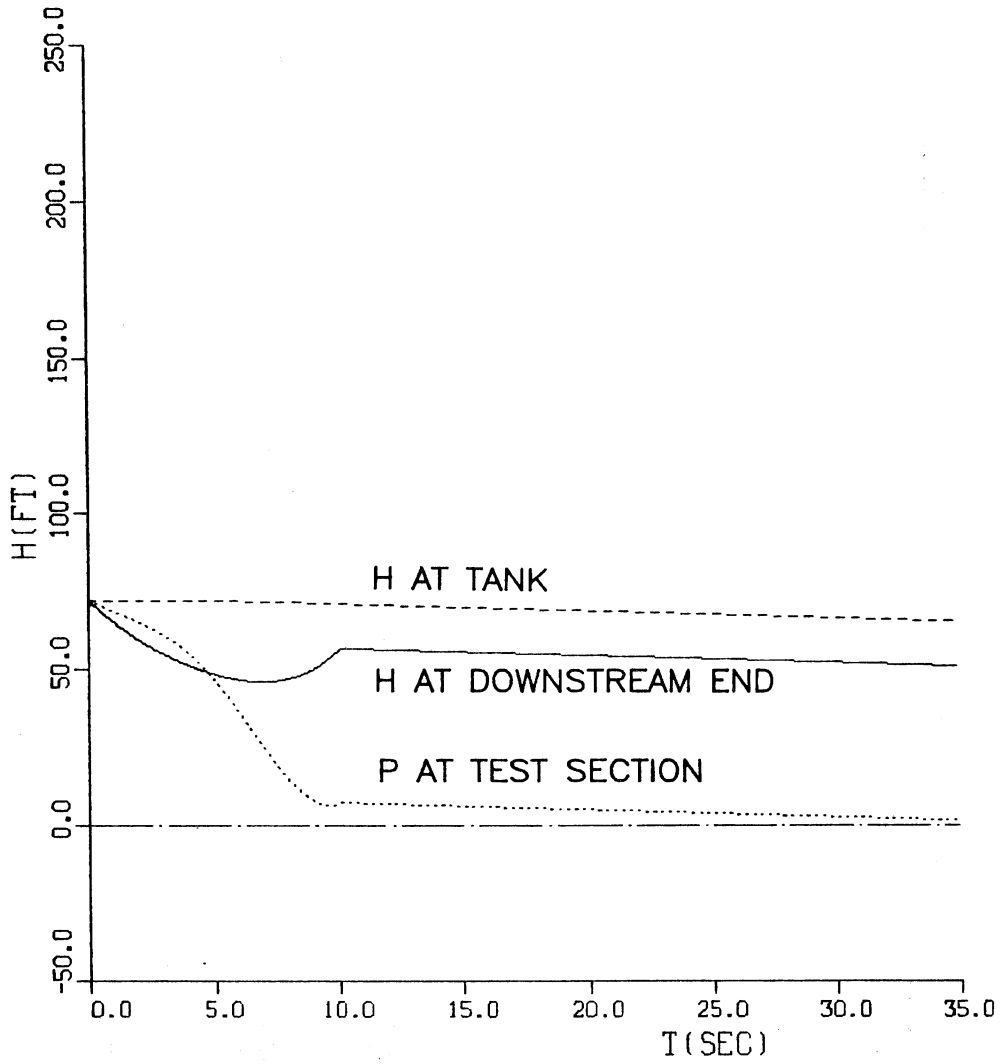

Figure 8. Hydraulic transient when the test section velocity is increased with continuous rate of change.

The time of flow establishment T_1 can be decreased somewhat if necessary. Figures 9 and 10 show the result of using T_1 = 5 seconds. A slight valve movement overshoot near the end of the 5 second period is needed. The accuracy of the solutions to the inverse problems described above were varified by comparing these solutions with the solutions of the corresponding direct problems. A corresponding direct problem is obtained by using the valve coefficient C_v calculated by the original indirect problem as the downstream end boundary condition.

B. Contraction

This section describes the performance of a contraction in a general configuration originally suggested by DTNSRDC as shown in Fig. 11. There is a long elbow with guide vanes directing the flow from the storage tank to the contraction. The contraction is assumed to be an axisymmetrical cylinder generated by a fifth order polynomial. It is 24 ft long contracting from 18 ft diameter to 2.25 ft. In calculating the flow, it is assumed that the elbow and guide vanes can produce a uniform velocity distribution at the contraction entrance. Under this condition, the flow is axisymmetrical and only a typical small region spanned by one $\Delta\theta$ needs to be considered. A typical grid-system on the x-r plan is shown in Fig. 12.

Because the fifth order polynomial has one extra degree of freedom, three different cases with the length ratio L_d/L = 0.5, 0.6, and 0.7 are calculated. Figure 13 shows the pressure distributions along the wall and along the axis for the L_d/L = 0.5 case. Some of the computed flow quality parameters are listed in Table 1. Among the three alternatives, the last case, L_d/L = 0.7, gives best performance. The velocity at the test section is very uniform and no flow separation is likely to occur.

The model which assumes axisymmetric flow is not capable of calculating a general case of nonuniform velocity distribution at the contraction entrance. Thus this configuration strongly depends on a good design of the elbow and guide vanes. It appears that the design and construction of such an elbow and guide vanes may be very expensive.

C. Side Outlet

1. Geometrical Configuration

This section describes the design of an alternative contraction which is directly attached to the sidewall of the storage tank as sketched in Fig. 14. The contraction is basically an axisymmetric cone generated by rotating a third order polynomial.

$$r = a + bx + cx^2 + dx^3 \tag{28}$$

about the x-axis yielding a surface described by

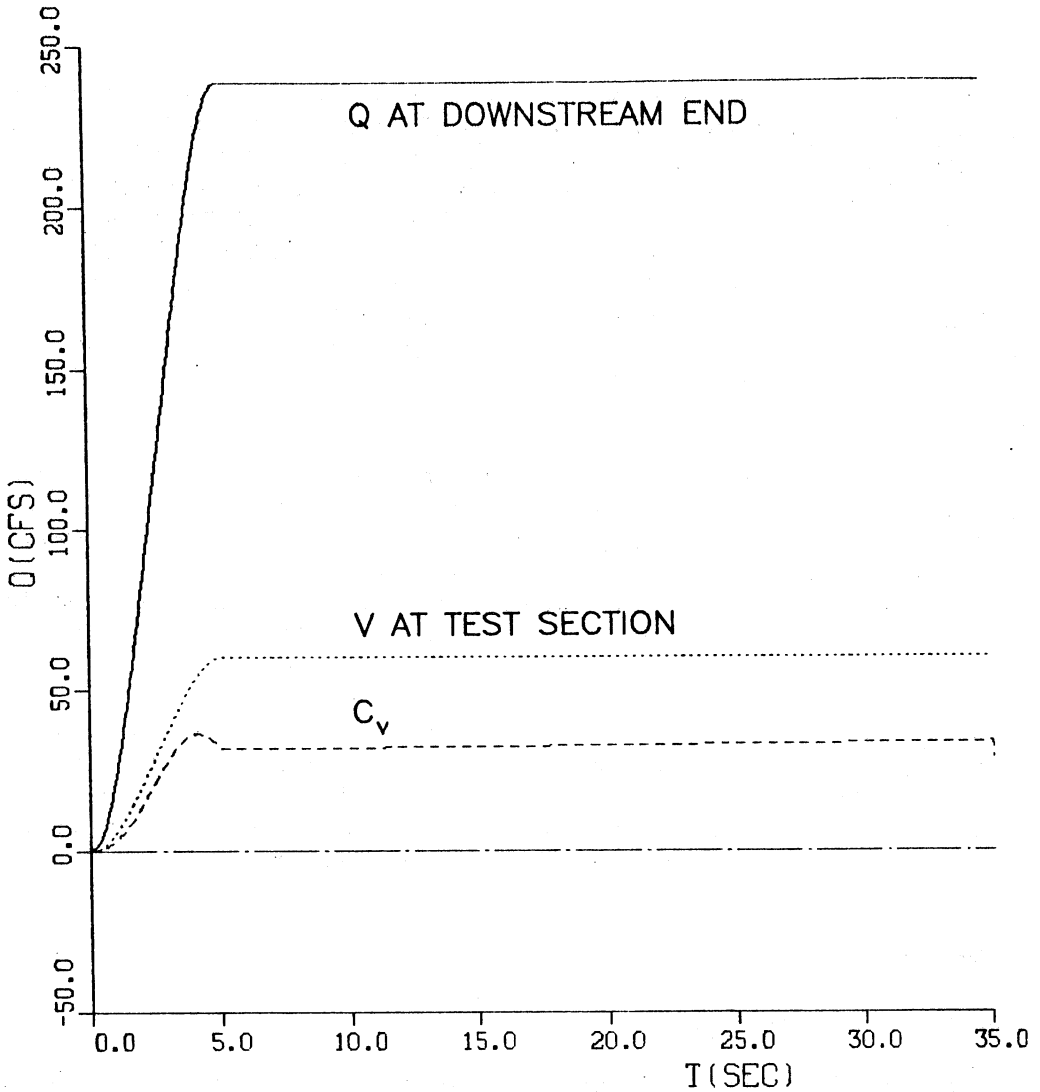

Figure 9. Hydraulic transient when the test section velocity is increased with continuous rate of change with time of flow establishment reduced to 5 sec.

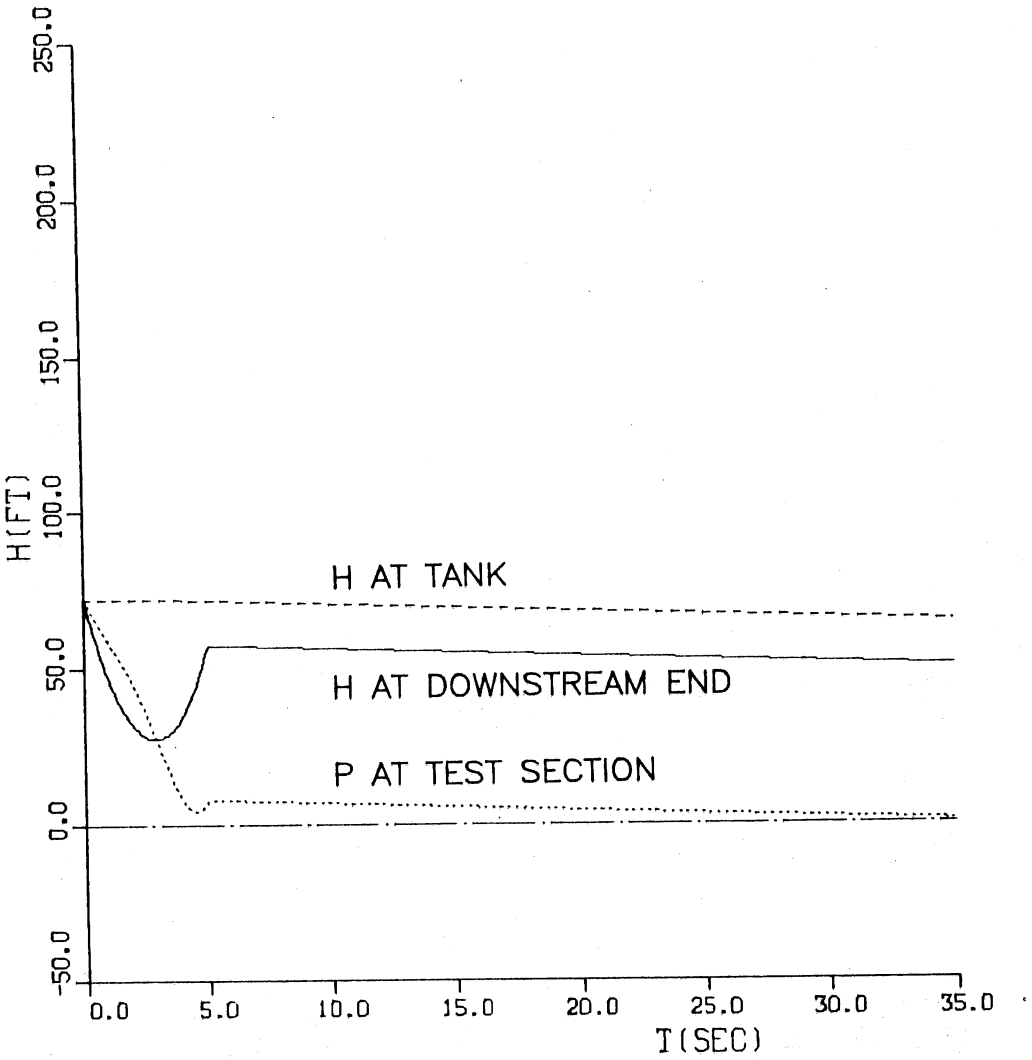

Figure 10. Hydraulic transient when the test section velocity is increased with continuous rate of change with time of flow establishment reduced to 5 sec.

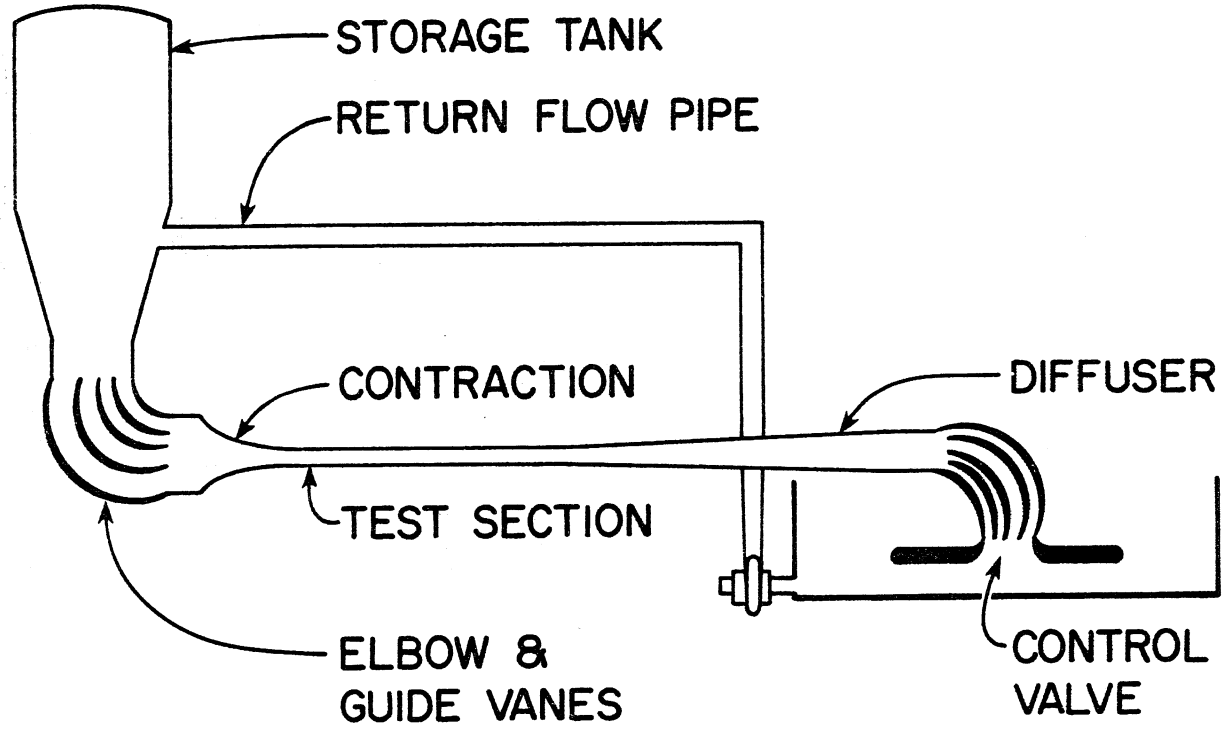

Figure 11. Original gravity flow facility design.

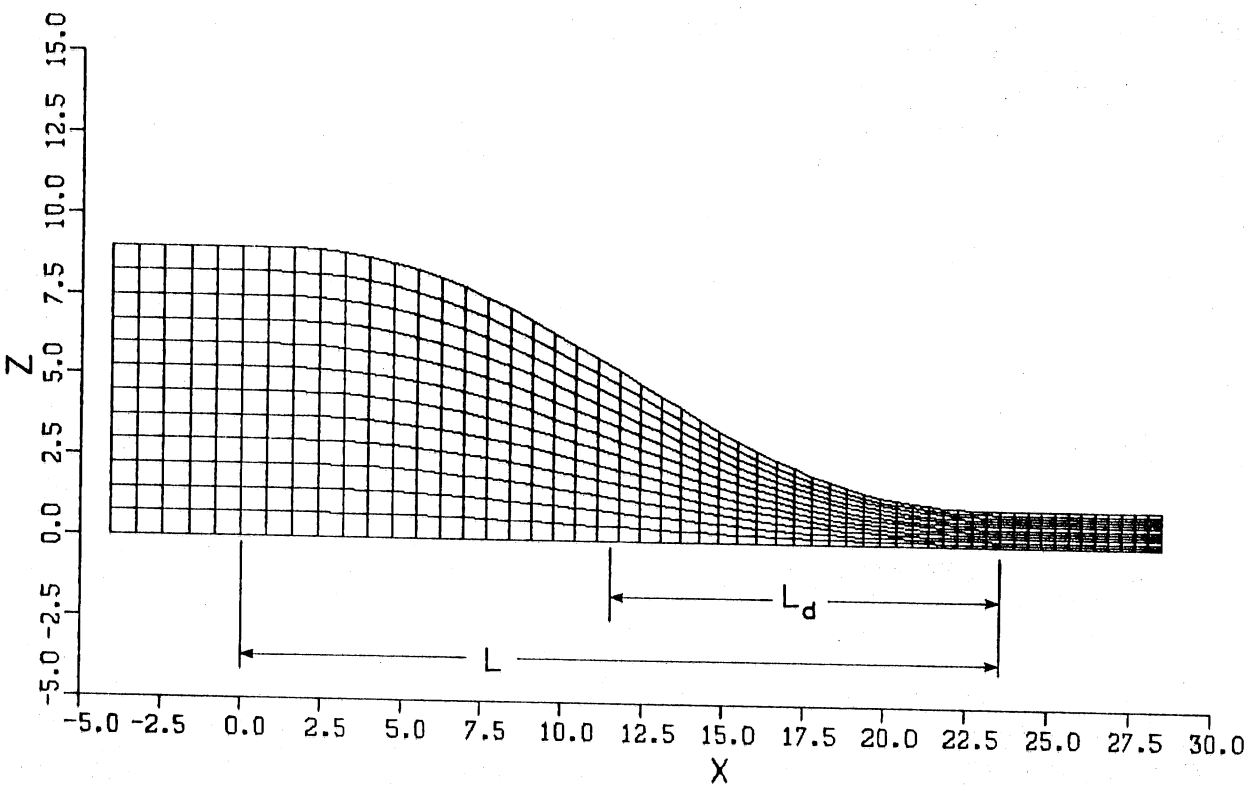

Figure 12. Typical grid system on x-r plane.

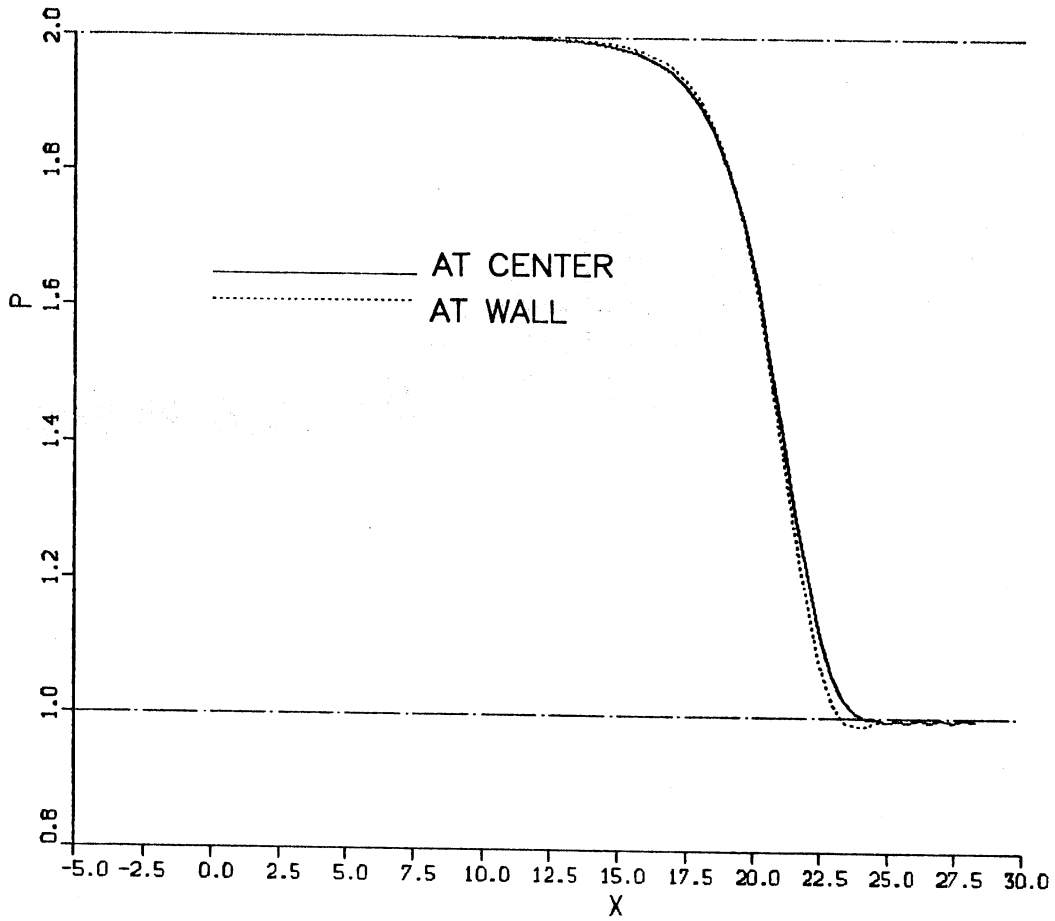

Figure 13. Pressure distribution in the contraction for $L_d/L = 0.5$ case.

TABLE I

Summary of Flow Quality Parameters

for Fifth-Order Polynomial Contraction

L_d/L	0.5	0.6	0.7
CP_{min}	.9878	.9886	.9921
X_{min}	L	L	L
CP_{max}	1.9997	2.0004	1.9999
X_{max}	0	0.27 L	0
U_{max}	1.0051	1.0033	1.0024
$\frac{u_{max}-u_c}{u_c}$	0.006	0.003	0.002

Notation:

L = contraction length

L_d = length between point of inflection and the exit end of the contraction

$CP_{min} = \frac{P_{min}}{\frac{1}{2}\rho U_c^2}$ = minimum dimensionless pressure

X_{min} = distance from entrance to point of minimum pressure

$CP_{max} = \frac{P_{max}}{\frac{1}{2}\rho U_c^2}$ = maximum dimensionless pressure

X_{max} = distance from entrance to point of maximum pressure

U_{max} = maximum velocity in test section

U_c = velocity at the centerline of test section

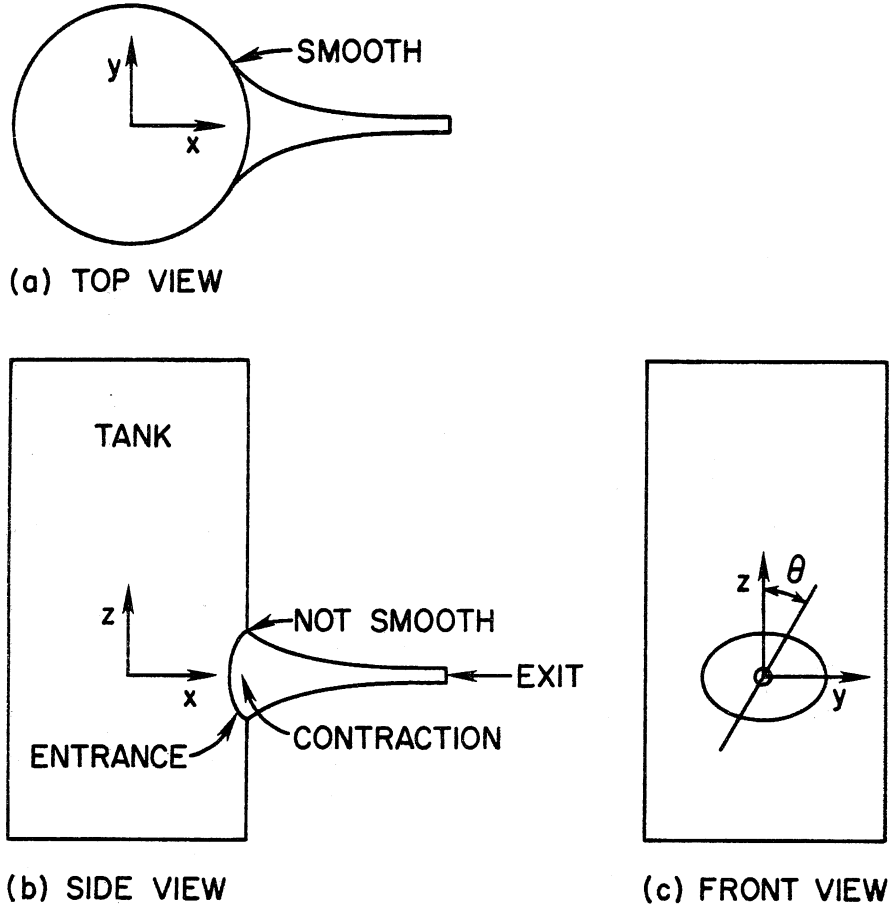

Figure 14. Tank-contraction connection alternative 1, without transition.

$$y^2 + z^2 = r^2 \tag{29}$$

The storage tank is a circular cylinder represented by

$$x^2 + y^2 = R^2 \tag{30}$$

where R is the radius of the tank.

Two alternative ways of connection between the contraction and the tank were analyzed. The first alternative is to join the third order polynomial contraction directly to the tank such that the nozzle will be tangent to the tank at only two points. The second alternative is to provide a short transition such that the contraction will meet the tank tangentially everywhere. These two cases are described in more detail.

a. Without transition

A third-order polynomial generated cone may be attached to a circular cylinder in such a way that the two surfaces intersect tangentially at two points on the x-y plane (horizontal plane) as shown in Fig. 14a. The two surfaces intersect each other at an angle greater than 180 degrees everywhere. The maximum angle of intersection occurs on the x-z plane (vertical plane) as shown in Fig. 14b. The contraction exit is made tangent to the test section minimizing the flow disturbance there.

The geometry of this contraction is uniquely determined or specified by a set of four parameters: tank diameter, diameter of the contraction entrance, test section diameter, and contraction length.

b. With transition

To avoid boundary layer separation and excessive vortex generation, it is desirable to have a smooth transition from the storage tank to the contraction. A simple way to achieve this is to add a short transition generated by a circular arc of variable radius between the tank and the original third order polynomial contraction. This transition section meets the third order polynomial cone tangentially on a vertical plane a certain distance away from the tank. The transition section also meets the storage tank tangentially everywhere. The equations for the transition and the contraction can be obtained as follows.

Consider a plane containing the x-axis and making an angle θ with the z-axis as shown in Fig. 14c. A point on this plane may be represented by the X-Y coordinates which are related to the original coordinate through

$$X = x \tag{31}$$

$$Y = z \tan \theta \tag{32}$$

This auxiliary plane cuts the cylindrical tank along an ellipse given by

$$\frac{X^2}{A^2} + \frac{Y^2}{B^2} = 1 \tag{33}$$

where

$$A = R \tag{34}$$

$$B = R\sqrt{1 + \cot^2\theta} \tag{35}$$

One quarter of this ellipse E, the transition profile T, and the contraction profile C are shown in Fig. 15.

The third order polynomial contraction C on this plane may be represented, in general, by

$$Y = a + bx + cX^2 + dX^3 \tag{36}$$

where the coefficients are yet to be determined. The circular arc of the transition T may be written, in general, as

$$(X - X_o)^2 + (Y - Y_o)^2 = R^2_T \tag{37}$$

There are seven parameters in Eqs. 36 and 37 that must be determined based on the following criteria.

(i) The test section radius is R_E.

(ii) The contraction entrance radius is R_o.

(iii) The contraction length is L_C.

(iv) The transition length is L_T.

(v) The contraction is tangential to the test section.

(vi) The transition intersects the contraction tangentially.

(vii) The transition intersects the tank tangentially.

The first five conditions determine the coefficients in Eq. 36 in terms of an undetermined parameter S. The resulting equation for the contraction may be written as

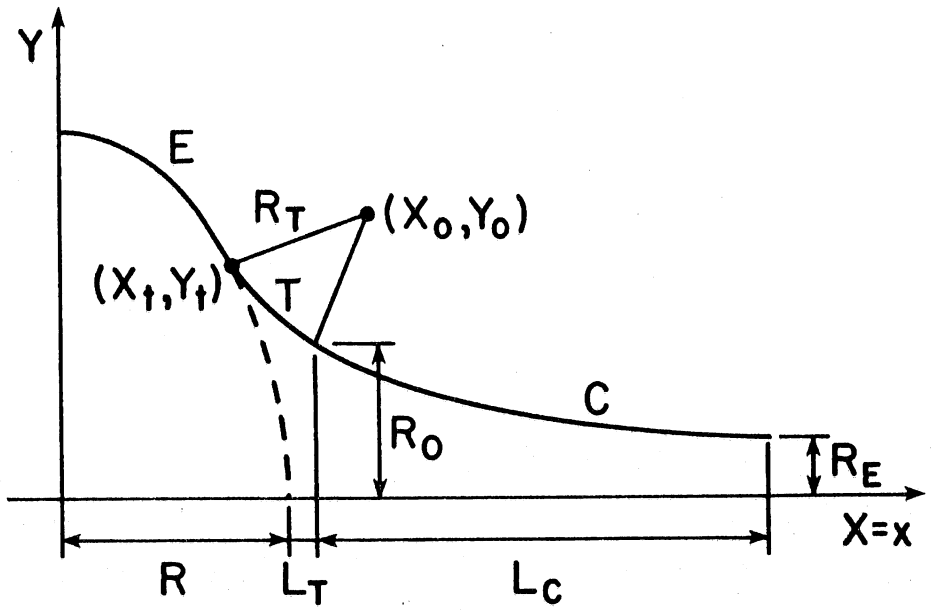

Figure 15. Boundary curves on x-y plane, $\theta \neq 0$.

$$\frac{Y-R_E}{R_o-R_E} = (3-S)\left(\frac{X-R-L_T-L_c}{L_c}\right)^2 + (S-2)\left(\frac{X-R-L_T-L_c}{L_c}\right)^3 \tag{38}$$

Here the parameter S is related to the slope of the tangent at the contraction entrance in the following way.

$$S = -\frac{L_c}{R_o-R_E}\left(\frac{dY}{dX}\right)_{X=R+L_T} \tag{39}$$

Condition (vi) actually represents two requirements. The first requirement that the point $(R+L_T, R_o)$ is on the circular arc T, leads to

$$(R + L_T - X_o)^2 + (R_o - Y_o)^2 = R_T^2 \tag{40}$$

The second requirement, the tangency requirement, leads to

$$\frac{R_o-R_E}{L_c} S \cdot \frac{Y_o-R_o}{X_o-R-L_T} = 1 \tag{41}$$

Let the coordinates of the point of tangency between the tank and the transition be (X_t, Y_t). Then, the following two equations must hold.

$$\frac{X_t^2}{A^2} + \frac{Y_t^2}{B^2} = 1 \tag{42}$$

$$(X_t - X_o)^2 + (Y_t - Y_o)^2 = R_T^2 \tag{43}$$

The last condition (vii) leads to the following equation.

$$\frac{B^2 X_t}{A^2 Y_t} = \frac{X_t-X_o}{Y_t-Y_o} \tag{44}$$

Thus far there are five constraining equations (Eqs. 40 - 44) and six unknowns (X_o, Y_o, X_t, Y_t, S, R_T). Therefore, there remains one more freedom of choice. One possible choice which is also the one adopted herein is to assume that the third order polynomial previously determined for the case without transition is retained. That is, the new contraction is obtained by replacing a small postion L_T as shown in Fig. 15 with a transition. This means S is determined from the known profile.

An alternative choice is to make the second derivative or the radius of curvature continuous at the junction between the transition and the third order polynomial. This condition leads to the following equation.

$$L_c^2\left[(Y_o-R_o)^2 + (R+L_T-X_o)^2\right] + (Y_o-R_o)^3(R_o-R_E)(8S-12) = 0 \qquad (45)$$

Since the radius of curvature at the entrance is an important parameter affecting flow separation at the entrance, it is logical to specify the minimum radius of the transition. In this case L_T may be regarded as an unknown. From Fig. 15, it is quite clear that the minimum R_T occurs when $\theta=0$. In this case $B\to\infty$ according to Eq. 35 and the ellipse E degenerates into a straight line X=R. Equations 42 and 44 simplify to

$$X_t = R \qquad (46)$$

$$Y_t = Y_o \qquad (47)$$

Equation 43 leads to

$$X_o = R + (R_T)_{min} \qquad (48)$$

where R and $(R_T)_{min}$ are specified quantities.

By eliminating X_o between Eqs. 40 and 41 and solving for Y_o , we obtain

$$Y_o = R_o + \frac{R_T}{\sqrt{1 + \dfrac{(R_o-R_E)^2S^2}{L_c^2}}} \qquad (49)$$

Equation 49 applies for any value of θ. For $\theta=0$, R_T is replaced by the known value of $(R_T)_{min}$. By substituting Eqs. 48 and 49 into Eq. 41 and solving for L_T we obtain:

$$L_T = (R_T)_{min}\left[1 + \frac{L_c}{\sqrt{L_c+(R_o-R_E)^2S^2}}\right] \qquad (50)$$

The solution procedure for the determination of the transition is as follows:

(i) L_T is calculated by Eq. 50 based on the known quantities $(R_T)_{min}$, S, etc.

(ii) The profile on the $\theta=0$ plane is determined by Eqs. 46-49.

(iii) For all other values of θ, we first determine B by Eq. 35.

(iv) Eqs. 40-44 are solved simultaneously for X_o, Y_o, X_t, Y_t and R_T. This completes the determination of the transition profile.

2. Grid Generation

Because the system is symmetrical with respect to the vertical plane containing the axes of the tank and the contraction, only half of the flow field was simulated. The assumption of flow symmetry reduces the computational load but, on the other hand, sacrifices the ability of the model to predict the possibility of an entrance vortex.

Figure 16 shows the simulated region and a schematic of how the grid system was generated. Basically, the region is first divided into two subregions. One subregion consists of the contraction and its extension into the tank and the other subregion is the remaining part of the tank. Therefore, there is an internal boundary common to the two subregions. The grids in the two subregions are so determined that they match on the internal boundary. An example of computer plotted mesh system is shown in Fig. 17. A fixed-grid system described in a previous section is used for the treatment of the free-surface boundary condition.

3. Numerical Results

The time dependent flow in the storage tank and the contraction was simulated for various tank diameters and other geometrical conditions. Initially the water is assumed to be stationary and the total head is equal to the piezometric head everywhere. At t=0 the piezometric head $P/\gamma+z$ at the exit is suddenly reduced to a smaller constant value to initiate the flow. Meanwhile the pressure on the free-surface inside the tank is maintained equal to the atmospheric pressure as the water surface elevation decreases. The unbalanced gravity force will accelerate the flow very rapidly to attain a quasi-steady flow condition within a very short time period. Although the flow will gradually slow down as the water level in the tank drops, its rate of change is so small compared with the speed of flow establishment that the attainment of flow establishment is easily recognizable.

For the purpose of illustration, some computer outputs for Run No. 10 are shown below. Figure 18 shows the velocity vector on the plane of symmetry. Note that different scales are used inside and outside the tank. Maximum dimensionless velocity inside the tank is 0.01883 and that inside the contraction is 1.151. Because of the limited tank size and the clearance between the tank bottom and the contraction, more flow enters

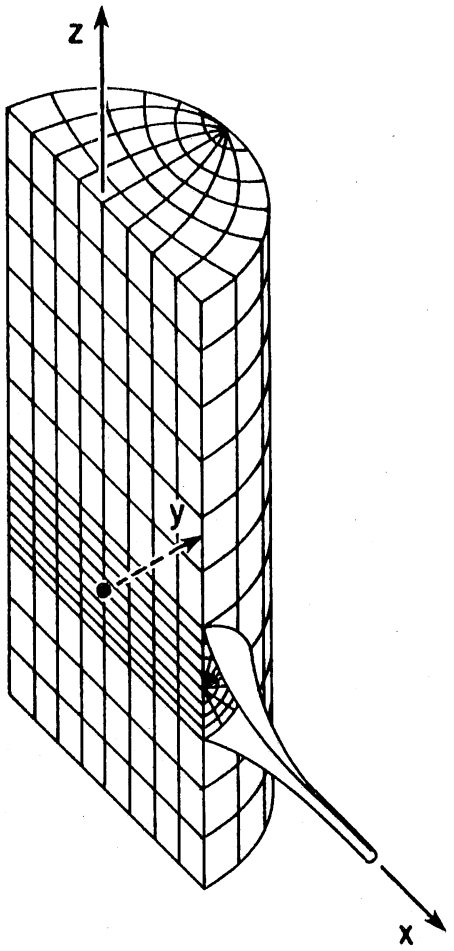

Figure 16. Schematic of tank-contraction grid system.

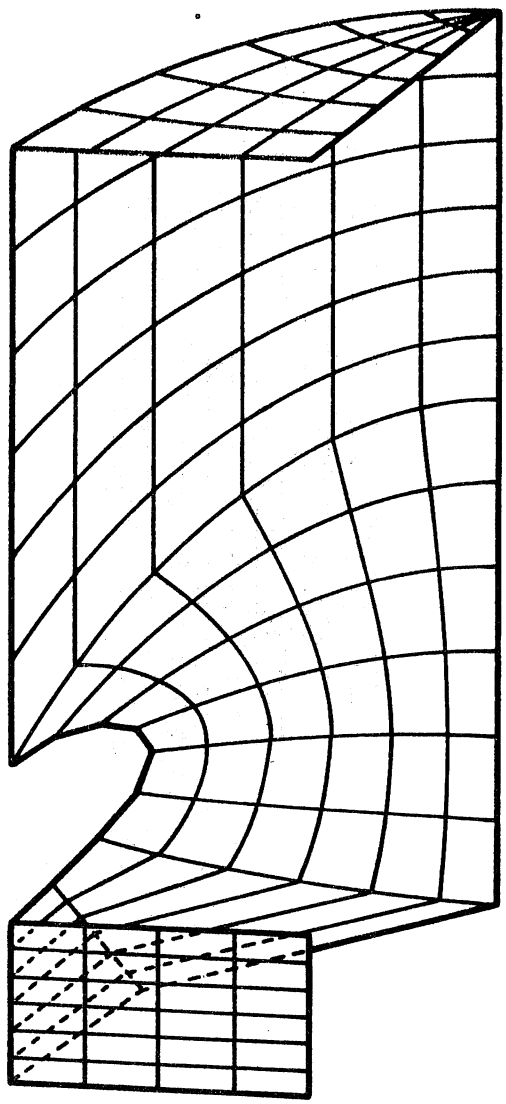

Figure 17a. Tank-contraction grid system.

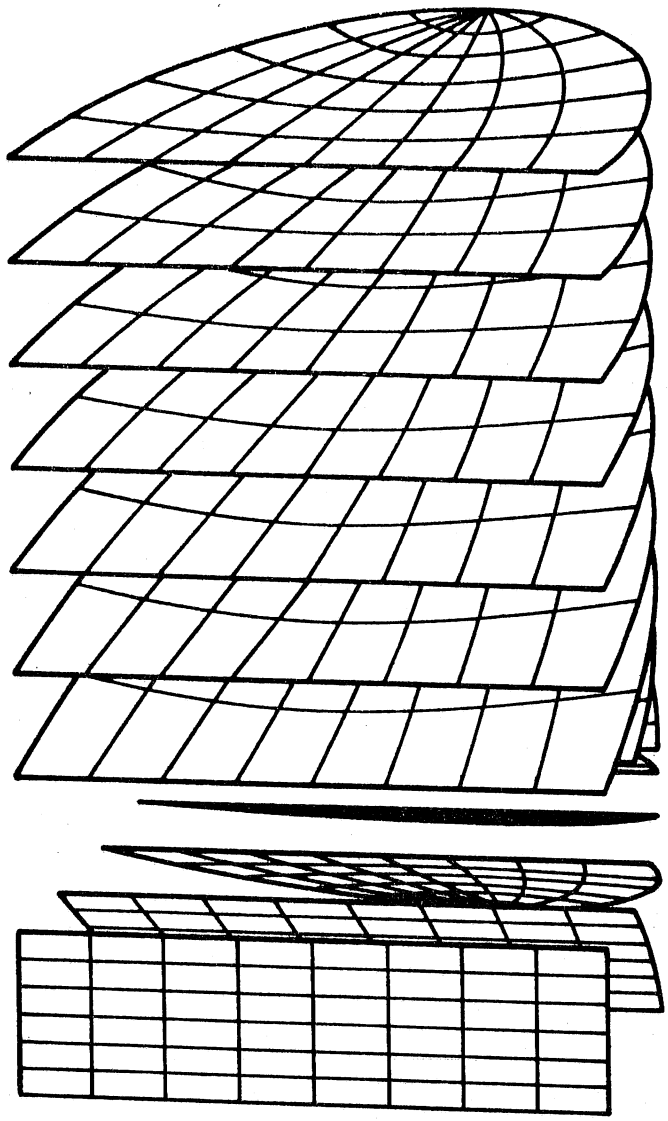

Figure 17b. Tank-contraction grid system.

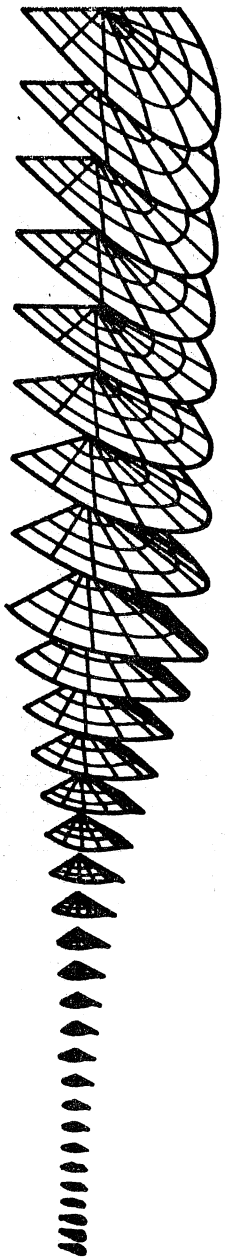

Figure 17c. Tank-contraction grid system.

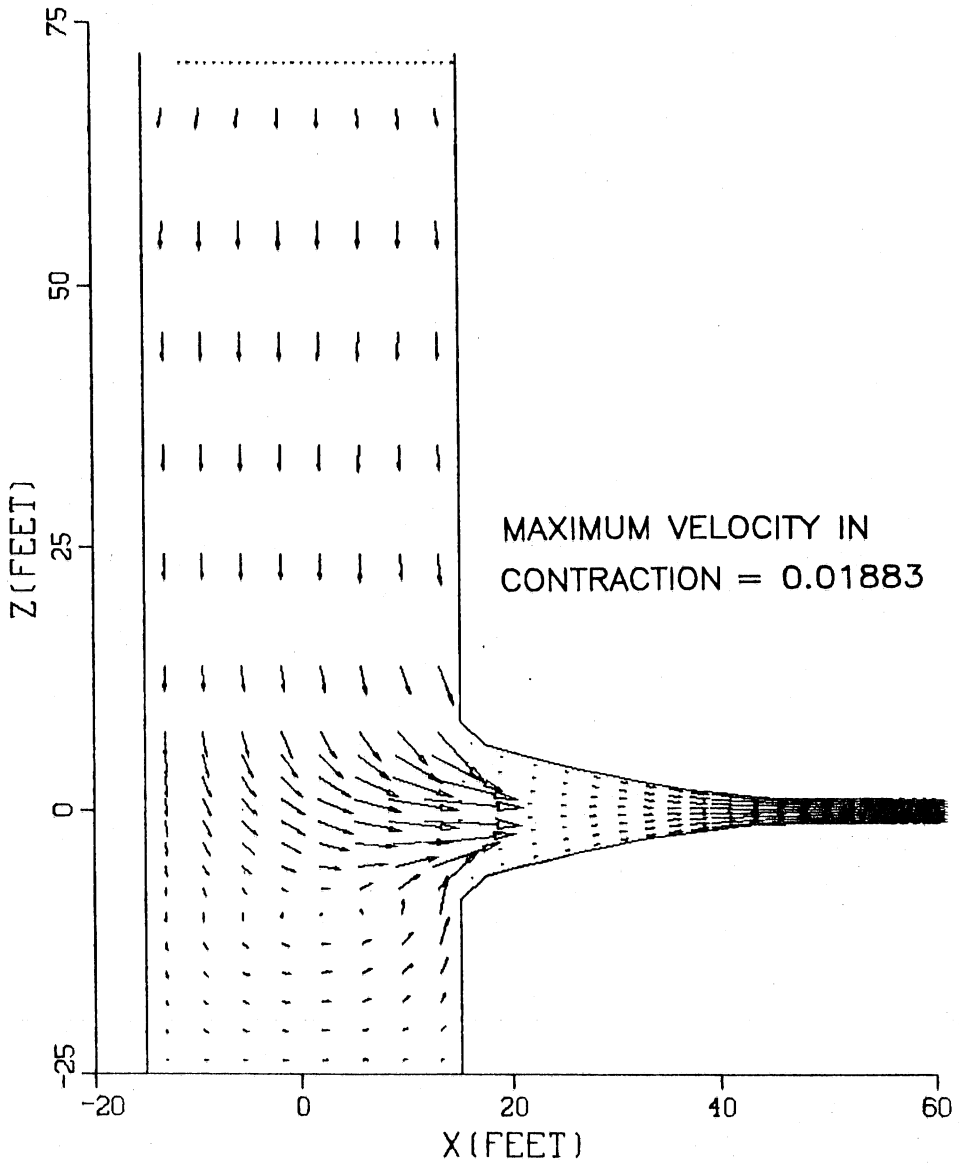

Figure 18. Velocity field on the plane of symmetry.

from above than from below at the contraction entrance. This slightly nonuniform velocity distribution at the entrance may affect the velocity distribution at the exit.

The velocity distribution at the contraction exit is shown in Fig. 19. Shown in the left half of the cross section are the isovel lines for the x-component of the velocity. The velocity vectors shown in the right half of the cross section represent the secondary current indicated by the y-and z- components of the velocity. There is a general downward (along the direction of gravity) movement of the magnitude approximately 0.1 percent of the horizontal velocity.

The velocity distribution along four different streamlines extending from the contraction exit to inside of the tank are plotted in Fig. 20. It shows that the velocity along the side is slightly greater than along the top, center, or the bottom of the contraction. The piezometric head, $P/\gamma+z$, distribution along the same streamlines are plotted in Fig. 21. A slight oscillation around the contraction entrance needs to be further investigated. The grids used in this and other runs are too large to resolve the flow around the transition accurately. Time and funds prevented carrying out more detailed analysis of the flow in the transition zone.

Some significant numerical results of five successful runs are listed in Table II. Contraction ratio, contraction length, and the tank diameter all influence the velocity distribution at the test section. According to this nonviscous flow model, the uniformity of velocity distribution at the test section is enhanced by increasing any of these parameters. However, for real fluid flow a large contraction length produces a thick boundary layer and adversely affects the flow quality. That a large contraction ratio enhances the uniformity of the velocity distribution is a well known fact. The present analysis also revealed the importance of the tank size. A large tank diameter allows the water to enter the contraction uniformly from all directions: uniform inflow produces uniform outflow. Boundary layer flow computations based on the computed pressure distribution indicate that the downstream part of the contraction is separation free.

The possibility of flow separation at the entrance or in the transdition zone has not been adequately studied. This study should be carried out later when the choice of alternative configuration is made. This computation requires very small grids at the entrance where the radius of curvature is small. Another parameter which has not been adequately analyzed is the clearance between the contraction and the tank bottom. For all five runs listed in Table II, the distance between the contraction axis and the tank bottom was kept equal to 25 ft. A larger clearance coupled with larger tank diameter may improve the entrance velocity distribution.

D. Pneumatic Drive System

The possibility of using a pneumatic or pneumatic-gravity drive system rather than a pure gravity system was brought up near the end of this project. Because the idea is very attractive, a very rough preliminary analysis was carried out to determine its hydrodynamic feasibility. The system considered is schematically illustrated in Fig. 22. The transition-

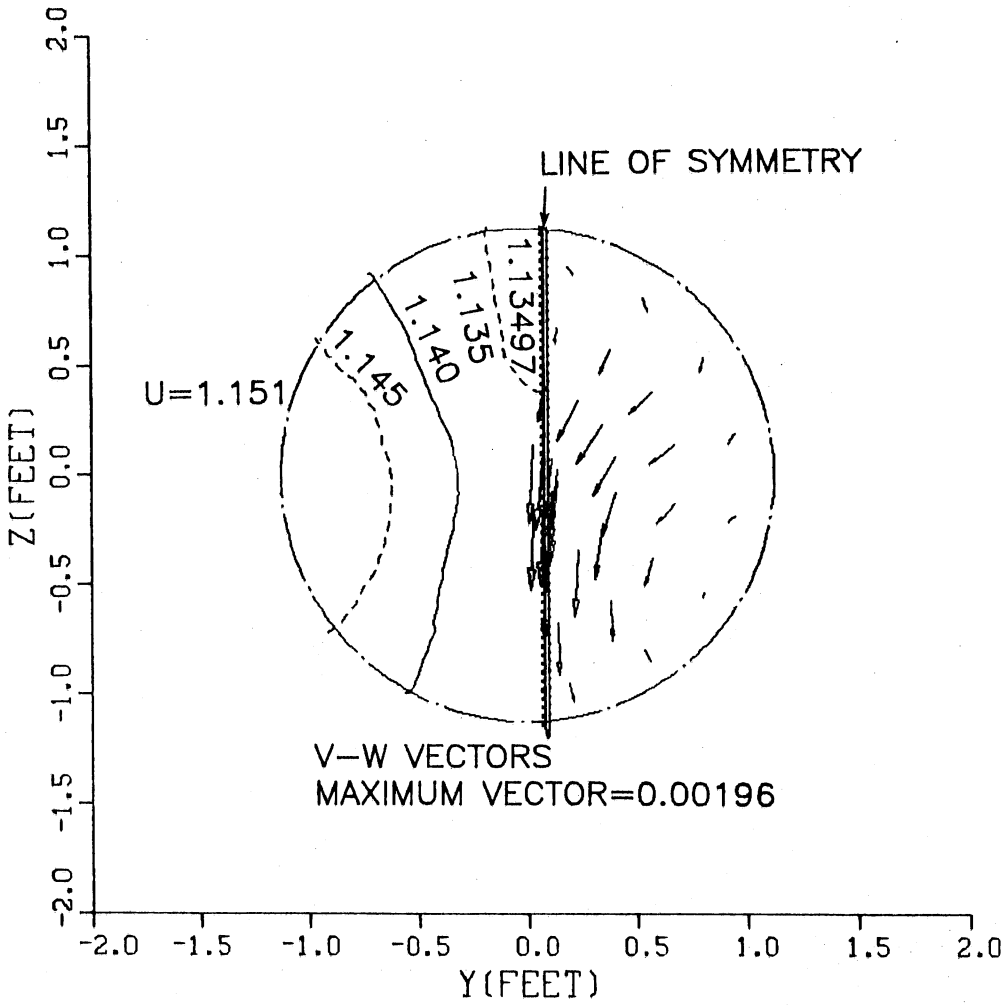

Figure 19. Velocity distribution at the contraction exit.

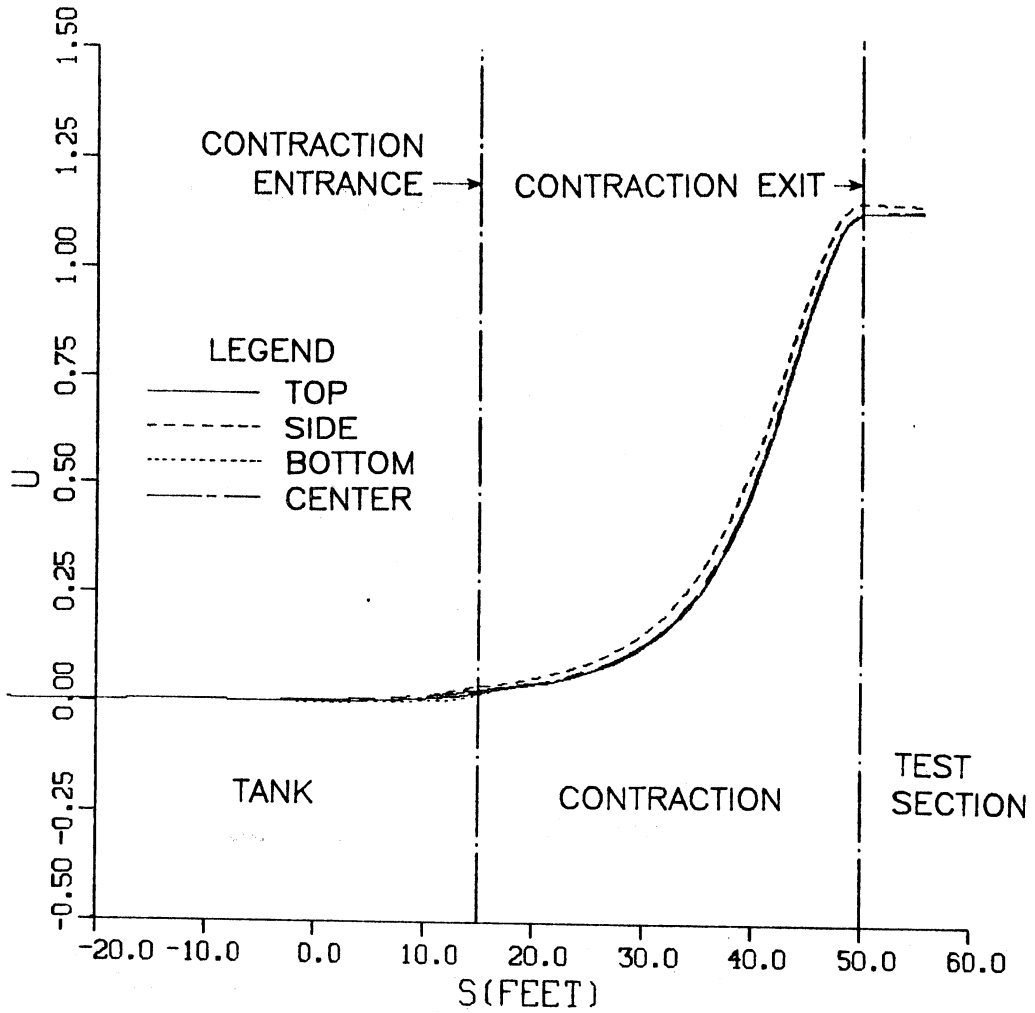

Figure 20. Velocity distribution along streamlines.

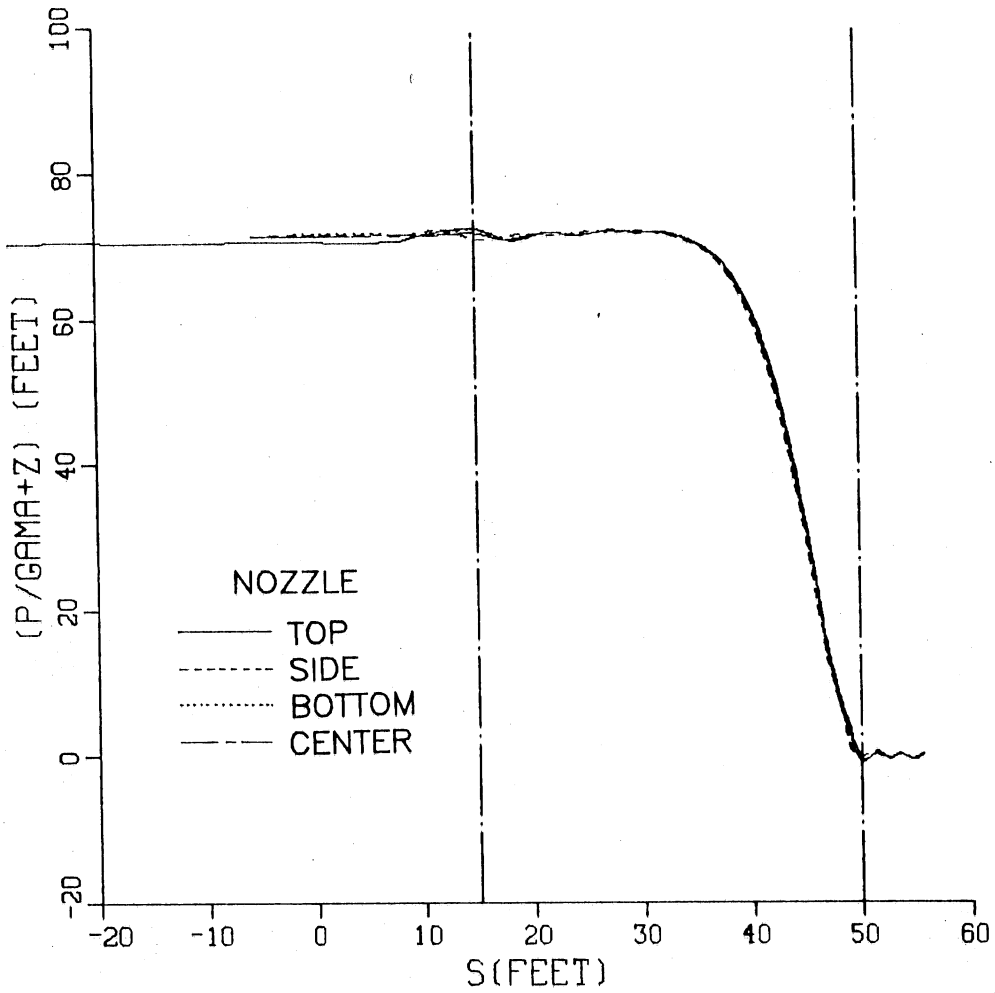

Figure 21. Peizometric head distribution along streamlines.

TABLE II

Summary of Runs for the Alternative

Design of Contraction and Transition

Run No.	7	9	10	11	12
Entrance Dia. (ft)	18.0	18.0	15.0	13.5	13.5
Exit Dia. (ft)	2.25	2.25	2.25	2.25	2.25
Contraction Ratio	64.0	64.0	44.4	36.0	36.0
Contraction Length (ft)	24.0	32.0	35.0	28.0	28.0
Tank Dia. (ft)	36.0	36.0	30.0	26.0	36.0
Transition Min R (ft)	No	No	2.0	2.0	2.0
Test Section					
$\frac{V_{max} - \bar{V}}{\bar{V}}$ %	1.15	0.85	0.95	1.35	1.10
Flow Separation in Contraction	No	No	No	No	No
Flow Separation at Transition	Likely	Likely	?	?	?
Exit V (fps)	60.0	60.0	60.0	60.0	60.0
Average V at Entrance (fps)	0.94	0.94	1.35	1.67	1.67
Average V in Tank (fps)	0.23	0.23	0.34	0.45	0.23

contraction-test section-diffuser part of this system is identical to that of the gravity system. The control valve located at the diffuser exit of the gravity system is not needed for the pneumatic system. The size of the upstream tank at the test section elevation, 36 ft according to Fig. 22, is dictated by the flow uniformity requirement. A larger size tank located at each end, 50 ft according to Fig. 22, represents the active storage requirement dictated by the flow rate and the testing time period. The dimensions shown in Fig. 22 are for illustration only. Compressed air is supplied to both storage tanks in a controlled manner.

The operational concept of the pneumatic system is described below:

(i) When the system is not in use (see Fig. 22), both tanks are opened to atmospheric pressure and the water surfaces are at equal elevation.

(ii) Preparation for test (see Fig. 23). Compressed air is directed to the lower tank to push water into the upper tank. The change in water surface elevation of H_1 causes the head difference due to gravity of $2H_1$. The pressure in the upper tank, Pu, may be adjusted to any value greater than the vapor pressure. A vacuum pump must be provided if below atmospheric pressure is desired.

(iii) Testing period (see Fig. 24). Air is simultaneously introduced into the upper tank and evacuated from the lower tank. The pressures P_u and P_d are varied such that the net head difference is kept constant.

$$\Delta H = \frac{Pu}{\gamma} + 2H_t - \frac{Pd}{\gamma} = K_1 \frac{V_t^2}{2g} \tag{51}$$

The pressure at the test section is

$$\frac{P_t}{\gamma} = \frac{P_u}{\gamma} + H_t + H_o - K_2 \frac{V_t^2}{2g} \tag{52}$$

By eliminating H_t from the above two equations, it is found that

$$\frac{P_t}{\gamma} = \frac{P_u + P_d}{2\gamma} + H_o + \left(\frac{1}{2} K_1 - K_2\right) \frac{V_t^2}{2g} \tag{53}$$

By properly adjusting the values of P_u, P_d, and H_o a desired set of values (V_t, P_t), within a certain range can be produced. There is, theoretically, no upper limit to P_t, but, there is a lower limit dictated by the value of H_o.

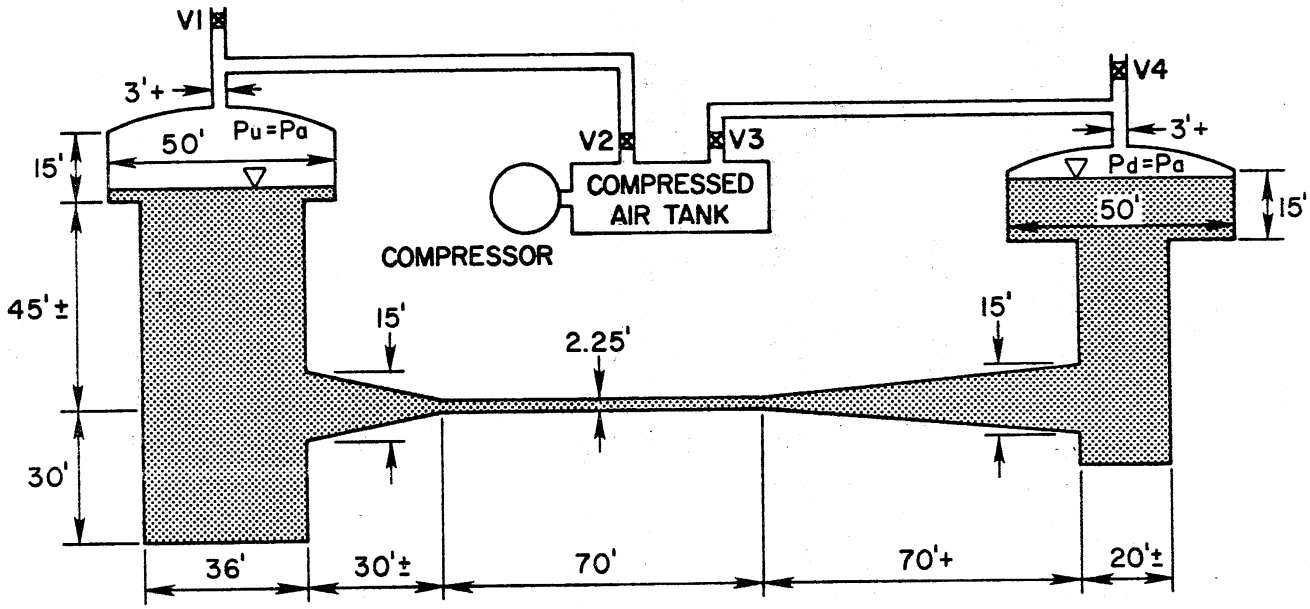

Figure 22. Schematic of a penumatic drive system - initial condition.

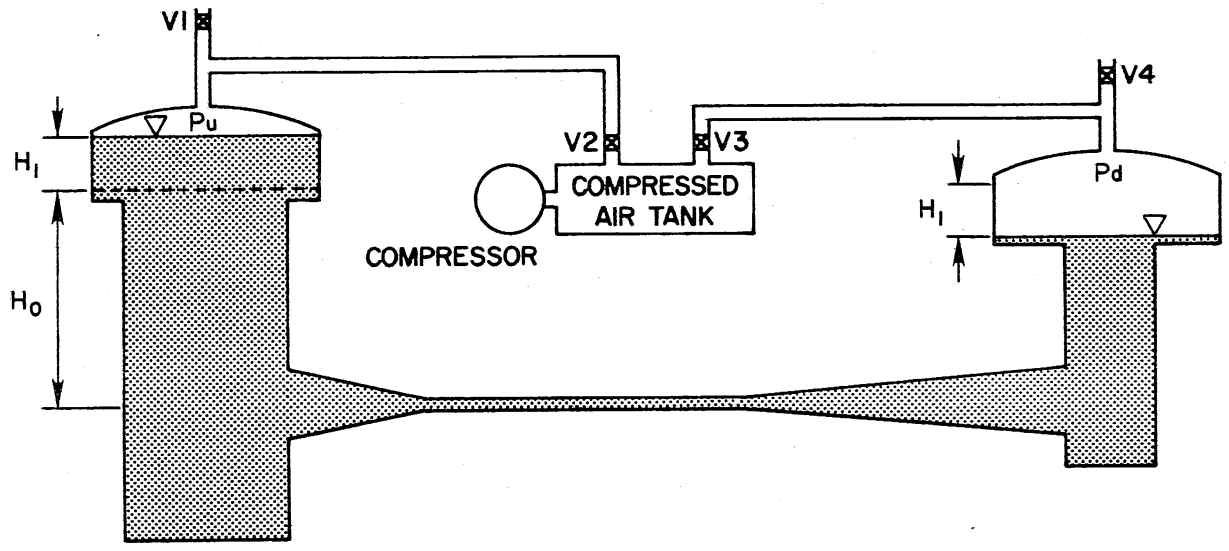

Figure 23. Preparation for test.

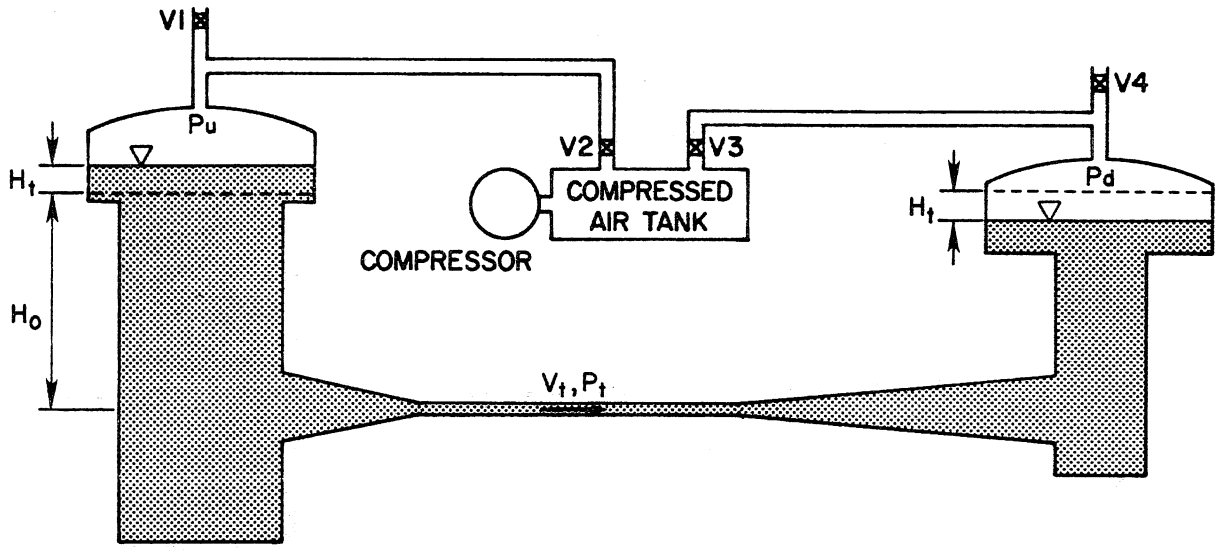

Figure 24. Testing period.

(iv) Stopping the test and preparing for next test (see Fig. 25). The flow must be stopped at the end of the test, reversed, and stopped again before the next test begins. A proper way of changing P_u and P_d must be found to minimize the overshoot and the subsequent disturbances as shown in Fig. 25.

The compressed air flow requirement was estimated using a quasi-steady flow calculation based on the assumption that the time required for the establishment of flow is 20 seconds and a constant test section velocity of 60 fps is to be maintained for 90 seconds. The required P_u and P_d variations and the corresponding volumetric air flow rates (Q_u and Q_d) are plotted as functions of time in Fig. 26. Note that the pressures change linearly with time. A sudden change in pressure and flow rate at time 20 seconds is not practical and undesirable. More accurate variations should be computed later using an unsteady flow model.

Maximum air flow rate of about 500 cfs as indicated in Fig. 26 is about twice that of the water flow rate. This means considerably large air ducts and a diffuser are needed to avoid generation of noise and prevent water surface disturbance.

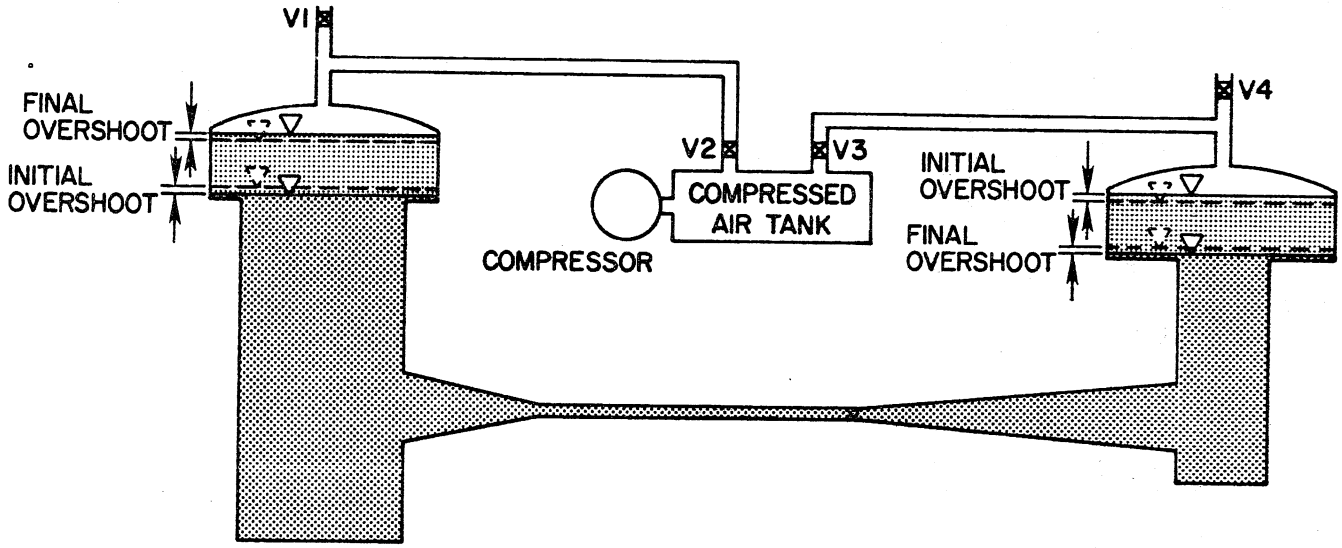

Figure 25. Stopping test test and preparing for next test.

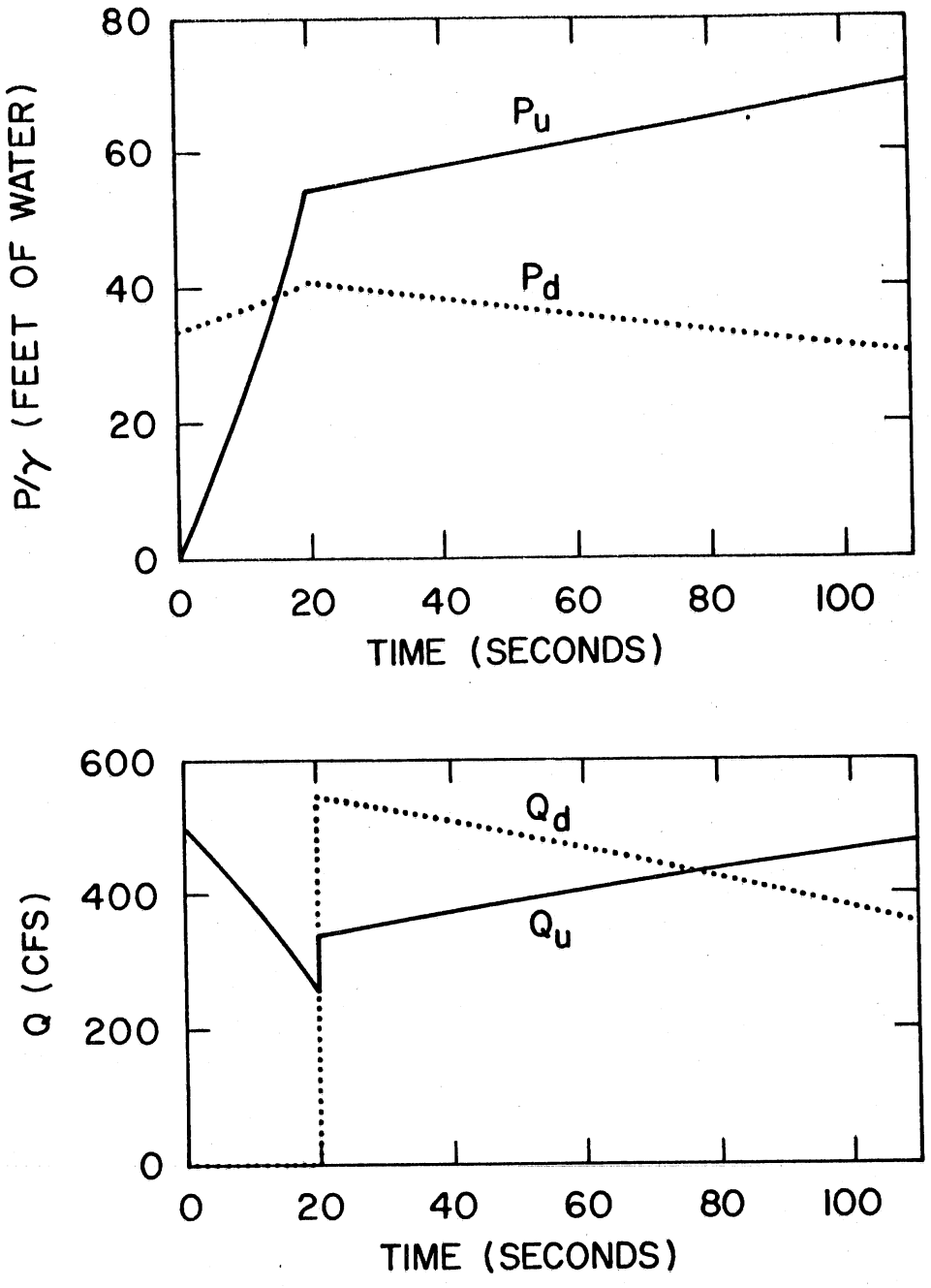

Figure 26. Estimated compressed air requirement.

IV. CONCLUSIONS

1. The gravity system and the pneumatic systems studied are both feasible alternatives. Each has hydrodynamic advantages and disadvantages.

2. The gravity system has the advantage of being simple to operate and has a relatively short response time to control command. Its main disadvantage is being unable to maintain constant velocity and pressure at the test section simultaneously. If the test section velocity is kept constant, then the test section pressure decreases gradually as the water is drained.

3. The pneumatic system has the advantage of being able to fix the velocity and the pressure at the test section at any desired values within certain ranges. This system will require somewhat longer times to establish a flow.

4. The design of contraction-test section-diffuser part of the water tunnel is common to the two alternative systems.

5. It appears better to have the contraction directly attached to the side of the head tank (the alternative design) than to have it attached to a 90 degree elbow extending from the bottom of the head tank (the original design). The alternative design is recommended.

6. A third order polynomial contraction of approximately 30 feet in length is needed. A short transition is needed to provide a smooth transition between the head tank and the contraction. The surface of the transition is generated by rotating a circular arc of variable radius of curvature about the axis of the test section. In this way, the first derivative is made continuous between the head tank and the transition. It is possible to make both the first and the second derivatives continuous at the transition-contraction junction and at the contraction-test section junction.

7. A pneumatic system is recommended because of its ability to control both velocity and pressure.

8. More detailed analysis and design is needed if a pneumatic system is chosen.

9. More detailed flow analysis in the transition region is needed to ensure a separation and eddy-free design.

10. Additional analysis is also recommended to assure that no intake vortex will be generated at the minimum submergence. This is especially important for a pneumatic system because the intake has a rather small submergence.